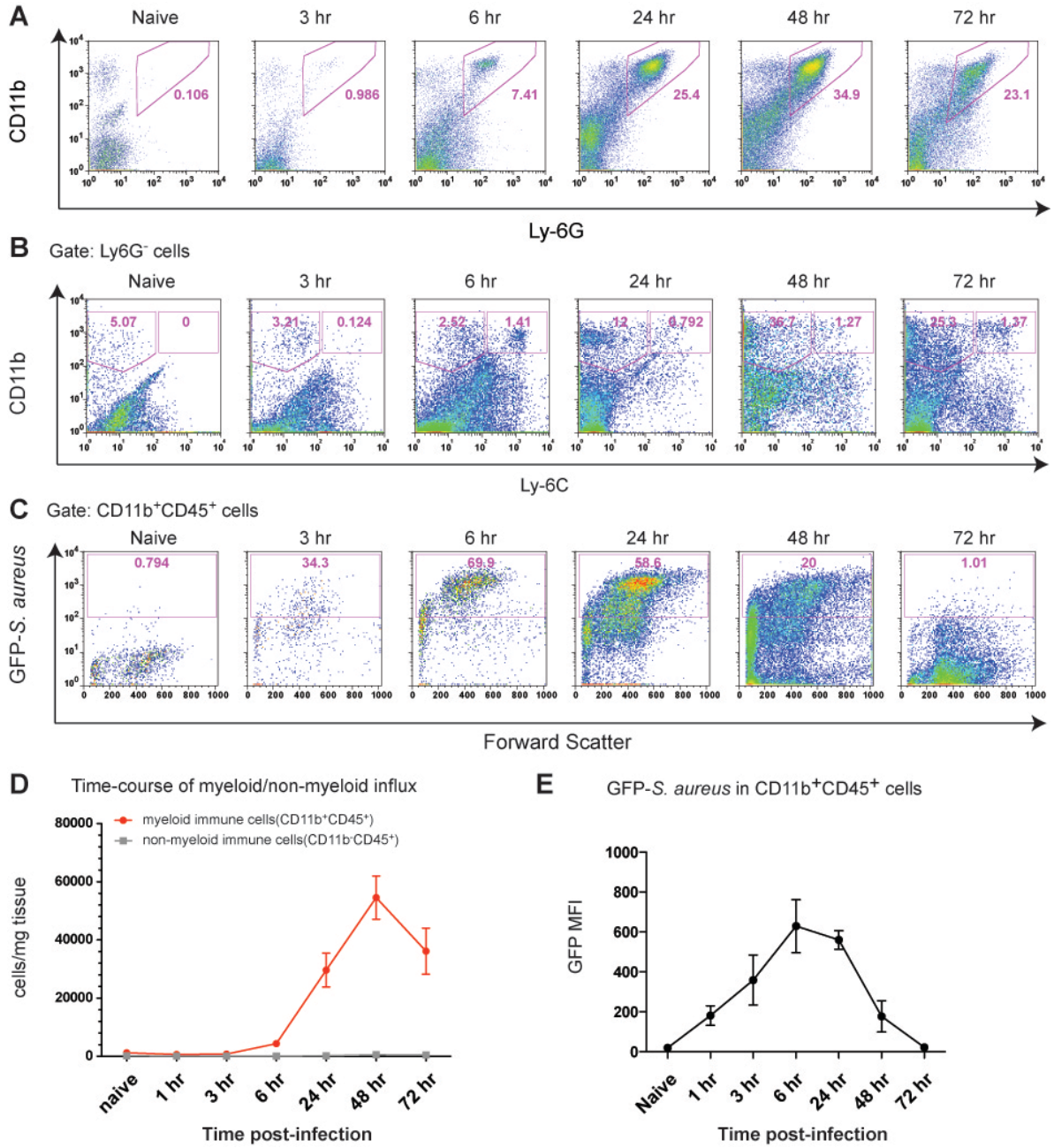

Supplemental Figure 1. Kinetics of immune cell influx in *S. aureus* infected paw tissue and myeloid cell ingestion of bacteria. (A) Flow cytometric plots of $CD11b^{+}Ly6G^{+}$ neutrophils (gates shown) in plantar tissues show increases at later post-infection time-points. **(B)** After gating out $Ly6G^{+}$ cells, $CD11b^{+}Ly6C^{hi}$ and $CD11b^{+}Ly6C^{lo}$ monocytes/macrophages are analyzed during infection (left and right gates, respectively). **(C)** Mice were infected with GFP-*S. aureus* ($5x10^{6}$ CFU): flow cytometry shows GFP within myeloid cells ($CD11b^{+}CD45^{+}$), reflecting ingestion of *S. aureus* at different time-points. **(D)** Determination of myeloid and non-myeloid immune cells in infected tissues shows myeloid cell peak at 48 hours. n=3 samples/time-point. **(E)** GFP-*S. aureus* mean fluorescence intensity (MFI, geometric mean) within myeloid cells peak at 6 hours. n=3 samples/time-point. Error bars, mean±s.e.m.

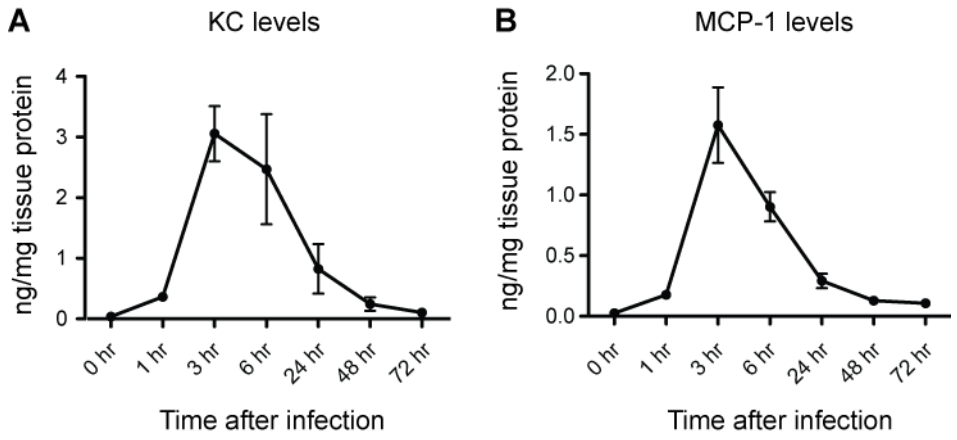

Supplemental Figure 2. Time-course of KC and MCP-1 levels in *S. aureus* infected tissues. Plantar paw tissue was isolated following infection with $5x10^6$ CFU *S. aureus*, homogenized and analyzed for **(A)** KC and **(B)** MCP-1 levels at different time-points using Luminex mouse cytokine beads. n=4 biological samples/time-point, values are normalized to total plantar tissue protein levels as measured by BCA assay. Error bars, mean±s.e.m.

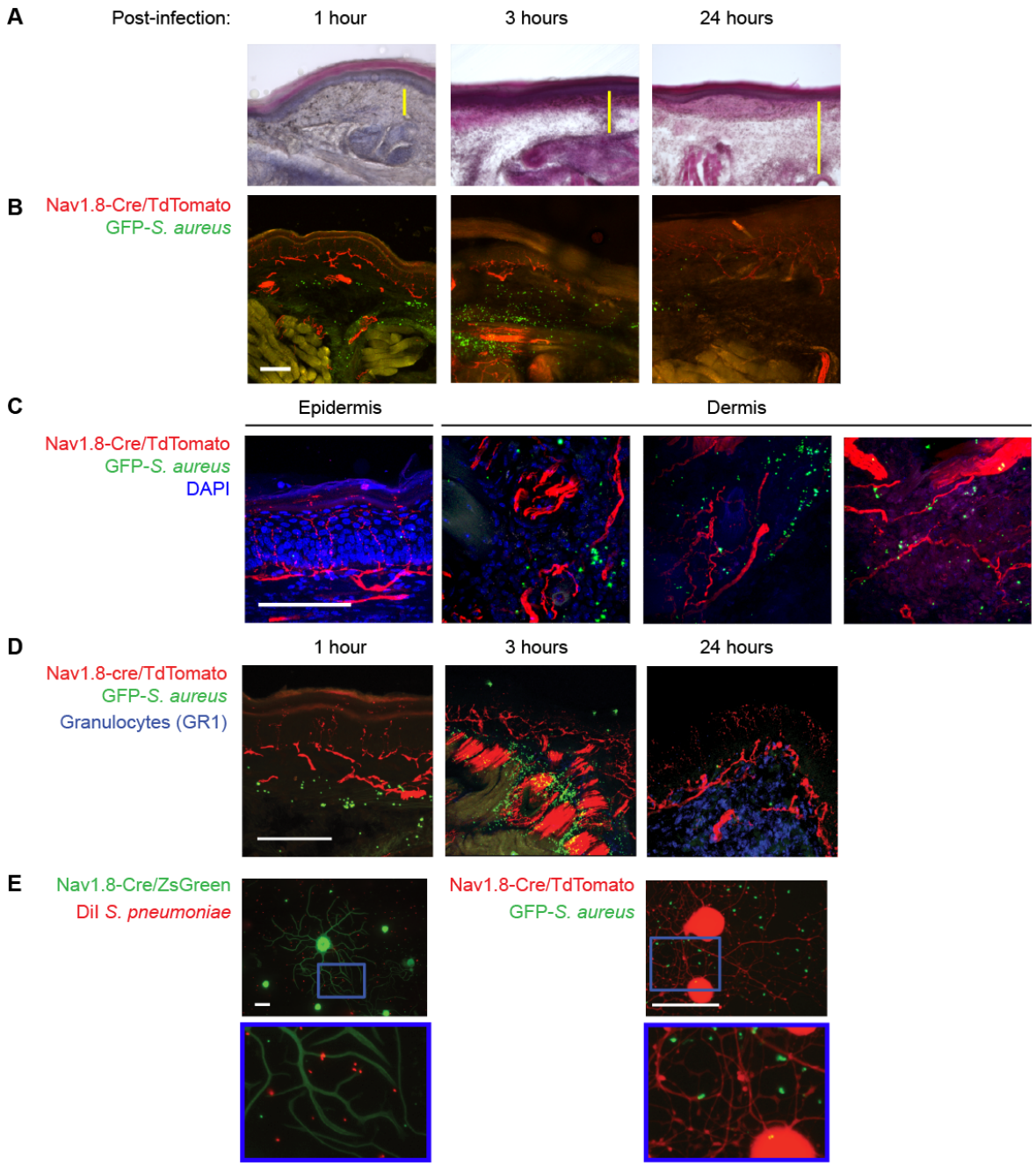

Supplemental Figure 3. Bacteria localize near nociceptive nerve fibers in infected tissues and neurites in co-cultures. (A) Hematoxylin/Eosin staining shows progressive tissue swelling between muscle and skin post-*S. aureus* infection (yellow lines). **(B)** Time-course of GFP-USA300 accumulation in Nav1.8-Cre/TdTomato mice following infection. **(C)** GFP-USA300 (green) were often juxtaposed to TdTomato nerve fibers (red) in dermal but not epidermal regions, 3 hours post-infection. **(D)** Anti-GR1 staining shows granulocyte populations appearing and fewer numbers of GFP-USA300 by 24 hours post-infection. **(E)** Nav1.8-Cre/ZsGreen or Nav1.8-Cre/TdTomato DRG neurons were co-cultured with CMTMR-*S. pneumoniae* (10^7 CFU, heat-killed) or 10^7 CFU GFP-*S. aureus* (10^7 CFU, live). Cultures were fixed and imaged-fluorescent bacteria were often in proximity to neurites. Scale bars, 100 µm.

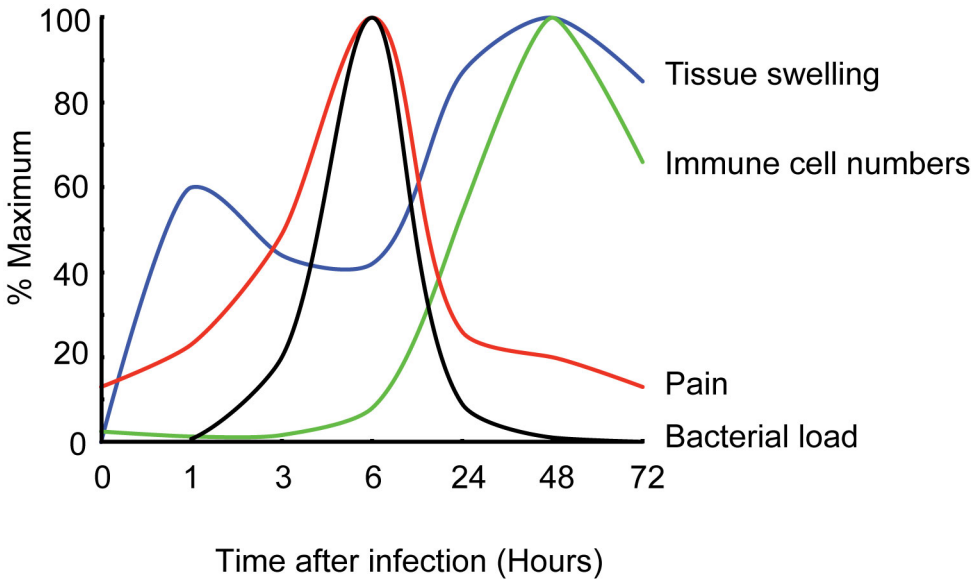

Supplemental Figure 4. Time-course of tissue swelling, immune cell numbers, pain and bacterial load following *S. aureus* infection. For pain, mechanical Von Frey thresholds were converted to inverse values. Each parameter was normalized to maximum values and connected by smoothened extrapolation. Pain correlates well with live bacterial load, and not immune cell numbers or tissue swelling.

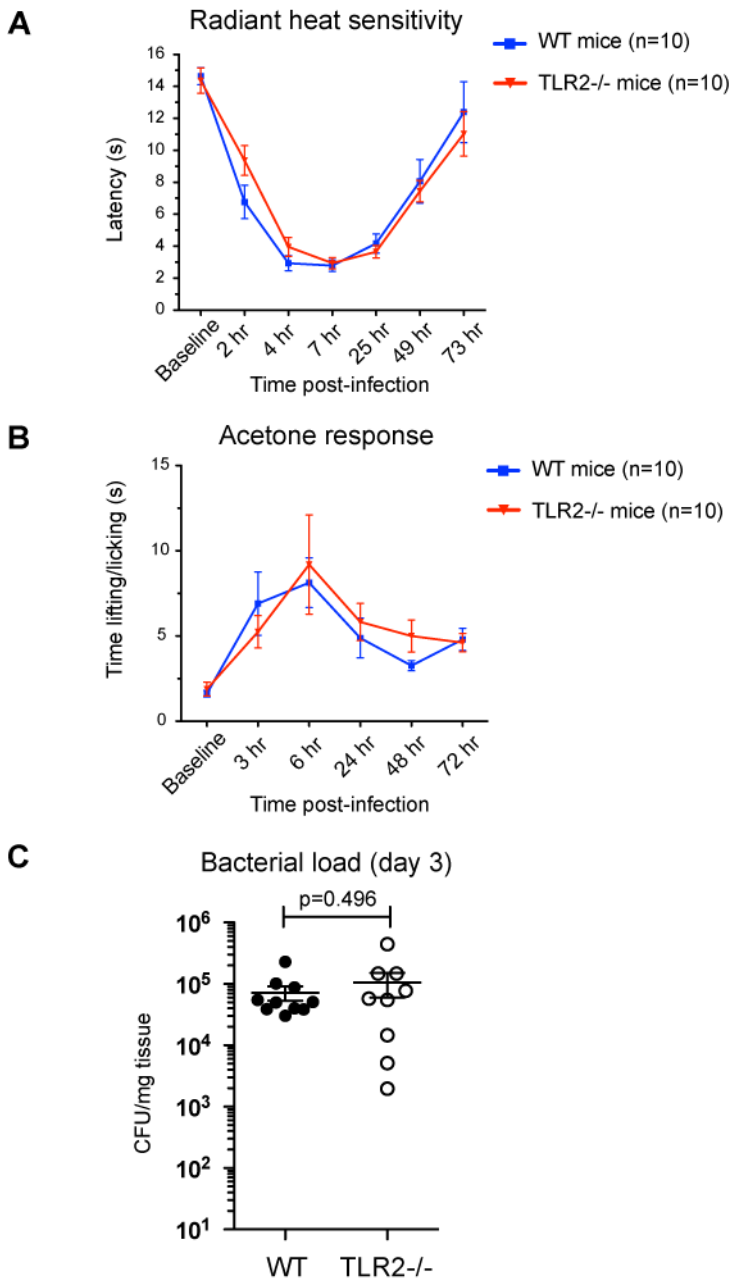

Supplemental Figure 5. TLR2 deficiency does not contribute to *S. aureus* induced heat or cold hypersensitivity. (A-B) Mice infected with $5x10^6$ CFU of LAC *S. aureus* were tested for heat and cold (acetone response) sensitivity. $TLR2^{-/-}$ and WT controls follow a similar time-course in the induction and resolution of hyperalgesia. Error bars, s.e.m. **(C)** Bacterial load of *S. aureus* in $TLR2^{-/-}$ and WT paw tissue show similar levels at 73 hr. post-infection (p-value, t-test). Error bars, mean±s.e.m.

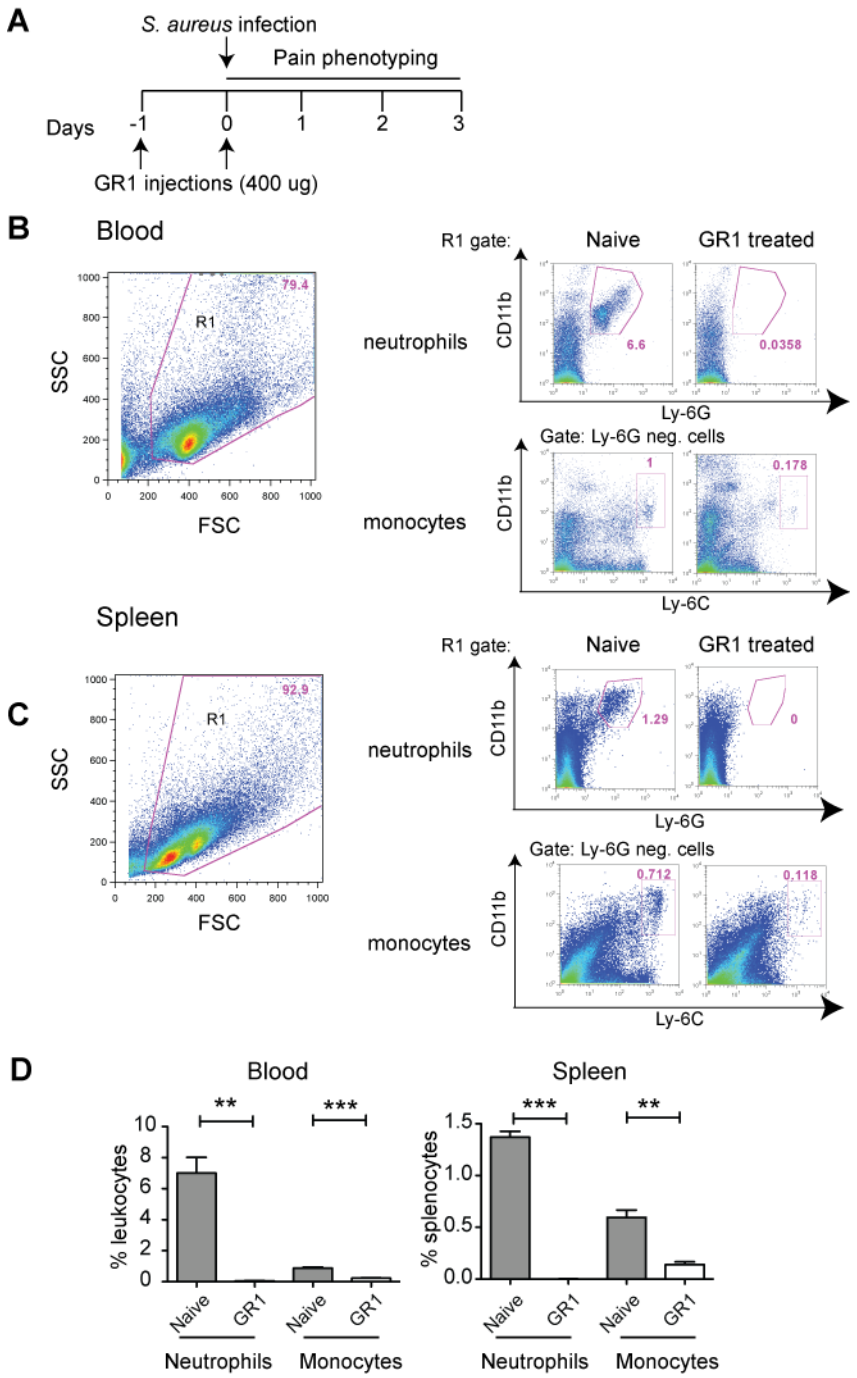

Supplemental Figure 6. GR1 antibody treatment eliminates blood-borne and splenic neutrophils, monocytes. (A) Injection scheme for GR1 treatment: 400 µg of GR1 or control antibody was injected i.p. 24 hours and one hour before live *S. aureus* infection. **(B)** Flow cytometry of blood and splenic cells from untreated mice or mice treated with GR1 at 24 hours post-treatment. CD11b, Ly6G, Ly6C staining shows depletion of the neutrophil ($CD11b^{+}Ly6G^{+}$), monocyte ($CD11b^{+}Ly6G^{-}Ly6C^{+}$) populations. **(C)** Quantification of populations analyzed in B, showing significant depletion of blood and splenic neutrophil/monocytes (n=3 mice/group, **, $p<0.01$; ***, $p<0.001$ by t-test). Error bars, mean±s.e.m.

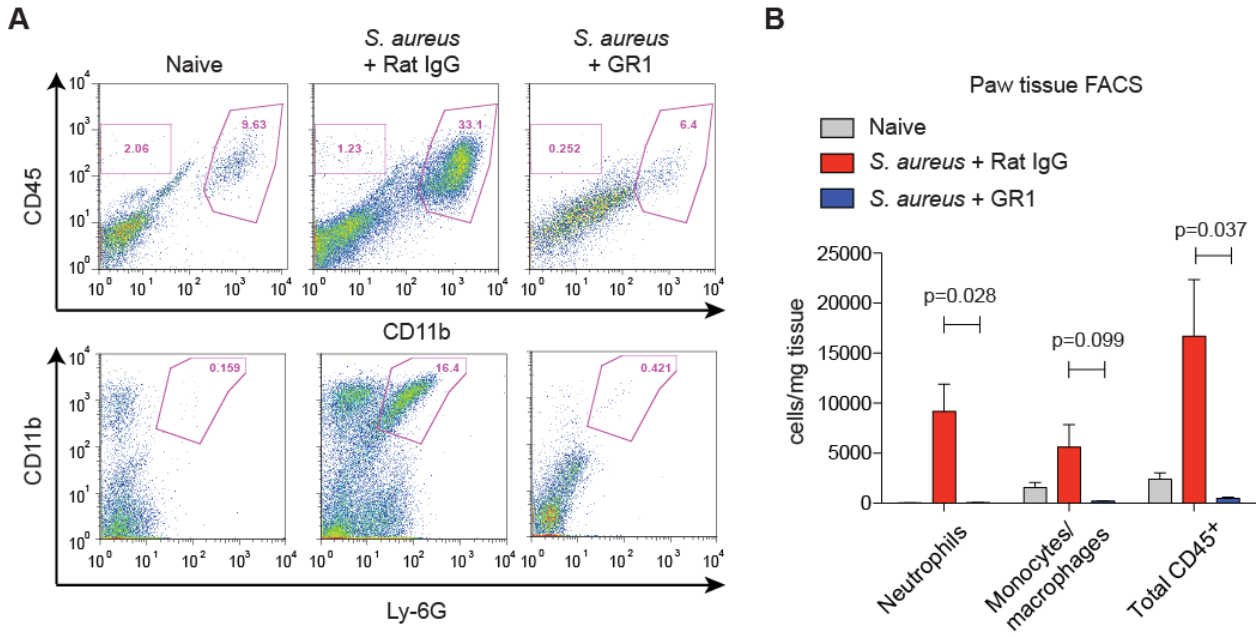

Supplemental Figure 7. GR1 treatment completely eliminates tissue infiltrating neutrophils and monocytes during *S. aureus* infection.
400 μg of GR1 or Rat IgG was injected i.p. 24 hours, one hour prior to intraplantar infection with LAC/USA300 ($5x10^6$ CFU). **(A)** Representative flow cytometry plots of infected paw tissue shows depletion of myeloid immune cells ($CD11b^+CD45^+$) and neutrophils ($CD11b^+Ly6G^+$) at 24 hours after *S. aureus* infection. **(B)** Quantification of infected tissue neutrophil ($CD11b^+Ly6G^+$), monocytes/macrophages ($CD11b^+Ly6G^-Ly6C^+$), and total immune cells quantified using the pan-immune marker, CD45, 24 hour post- *S. aureus* infection (p-value, unpaired, t-test). Error bars, mean±s.e.m.

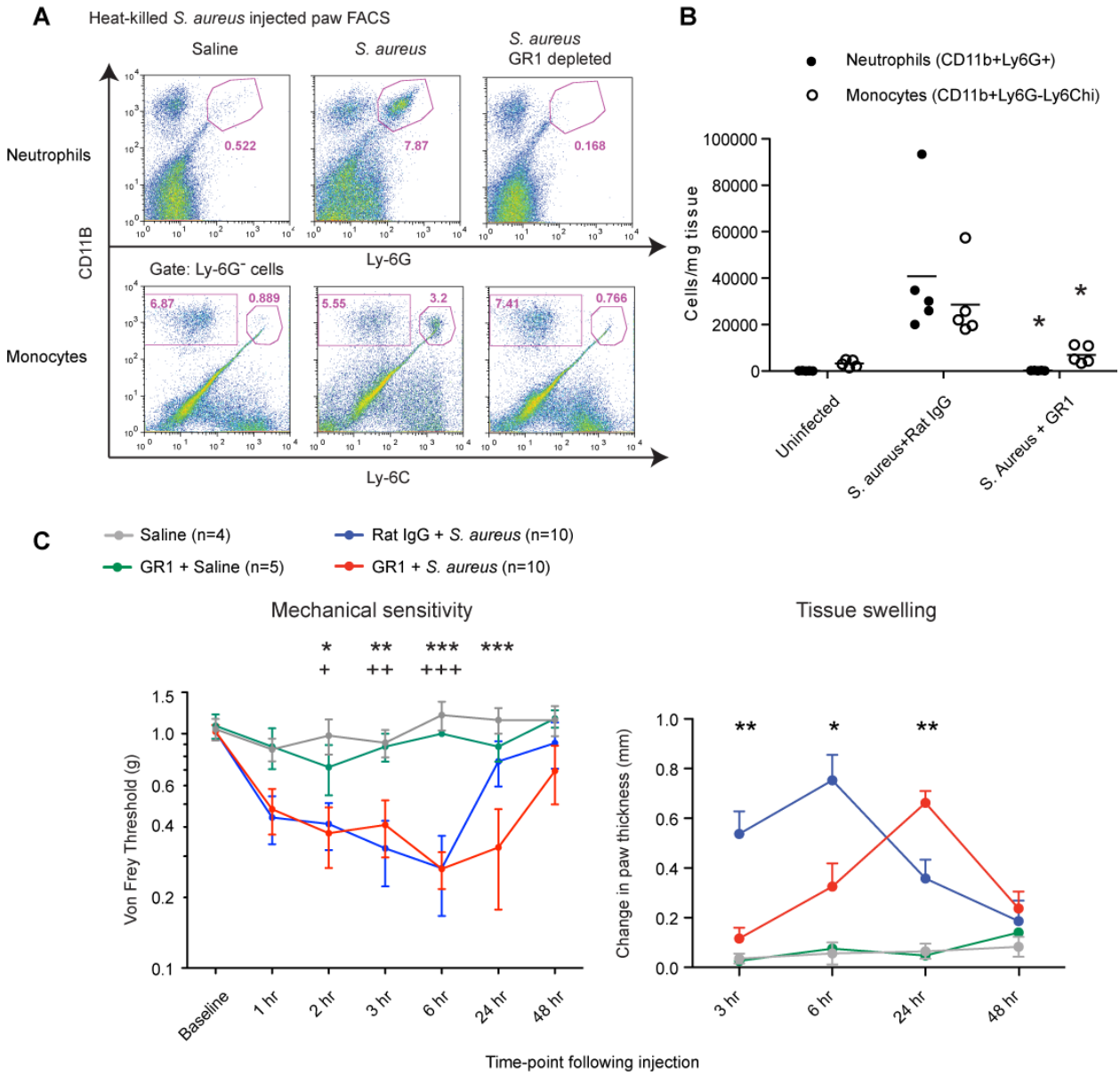

Supplemental Figure 8. GR1 treatment does not decrease pain caused by heat-killed (hk) *S. aureus*. Hk-*S. aureus* (10^8 CFU) was injected into the hind-paw: tissue swelling, plantar immune cell populations, and mechanical hypersensitivity were measured. Unlike live infection, hk-*S. aureus* induced Ly6C^{hi} monocytes rather than Ly6C^{lo} monocytes; pain also correlated with tissue swelling (see Fig. 1a). **(A-B)** GR1 or rat IgG (400 µg) was injected i.p. 24 hours, one hour prior to hk-*S. aureus*. Flow cytometry shows significant decreases in neutrophils, monocytes in plantar tissues 48 hr post-GR1 injection (5 mice/group; *, $p<0.05$, t-test, GR1 vs. rat IgG). **(C)** Mechanical hyperalgesia developed similarly in rat IgG and GR1 treated mice injected with *S. aureus*. (Bonferroni, *, $p<0.05$; **, $p<0.01$; ***, $p<0.001$ GR1 and hk*SA* vs. saline; +, $p<0.05$; ++, $p<0.01$; +++, $p<0.001$ Rat IgG and hk*SA* vs. saline). GR1 treatment significantly decreased swelling at 3, 6 hr, and caused more swelling at 24 hr, relative to rat IgG treated mice (Two-way ANOVA Bonferroni, *, $p<0.05$; **, $p<0.01$). Thus, GR1 treatment affects tissue swelling but not mechanical pain following hk-*S. aureus* injection. Error bars, mean±s.e.m.

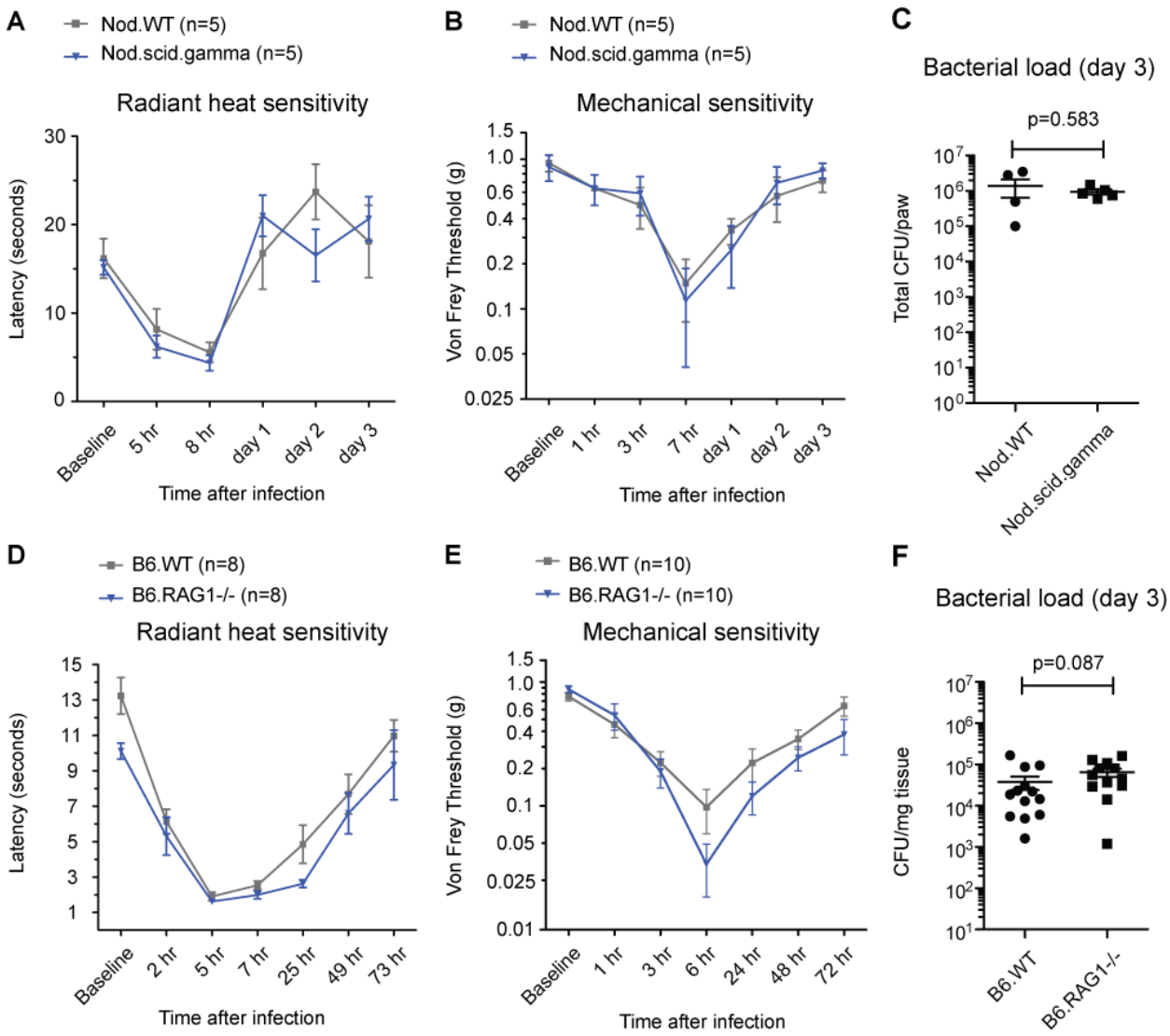

Supplemental Figure 9. Heat and mechanical hypersensitivity are not reduced in Nod.scid.gamma or B6.RAG1-/- mice following *S. aureus* infection.
In **A-C**, Nod.scid.gamma and Nod.WT mice, and in **D-F,** B6.RAG1$^{-/-}$ mice and B6.WT mice were tested for pain sensitivity following *S. aureus* infection (5x10^{6} CFU LAC). **(A-B)** No significant differences in heat hypersensitivity (p=0.314) were observed between infected Nod.scid.gamma and Nod.WT mice, or mechanical hypersensitivity (p=0.908, Two-way RM ANOVA). **(C)** *S. aureus* bacterial load did not differ significantly 3 days following infection (p=0.583, t-test, Nod.scid.gamma, n=5; Nod.WT, n=5) note: one Nod.WT sample was 0 CFU, so not displayed on axis). Behavioral analysis of the Nod mouse strain was challenging because of baseline hyperactivity despite repeated habituations. **(D-E)** No significant differences in heat (p=0.715, Two-way RM ANOVA) or mechanical hypersensitivity (p=0.198, Two-way RM ANOVA) were observed between *S. aureus* infected B6.RAG1$^{-/-}$ and B6.WT mice. **(F)** Bacterial load was slightly but not significantly increased in B6.RAG1$^{-/-}$ mice compared to B6.WT mice day 3 after *S. aureus* infection (p=0.087, t-test; B6.RAG1$^{-/-}$, n=12; B6.WT, n=13). Error bars, mean±s.e.m.

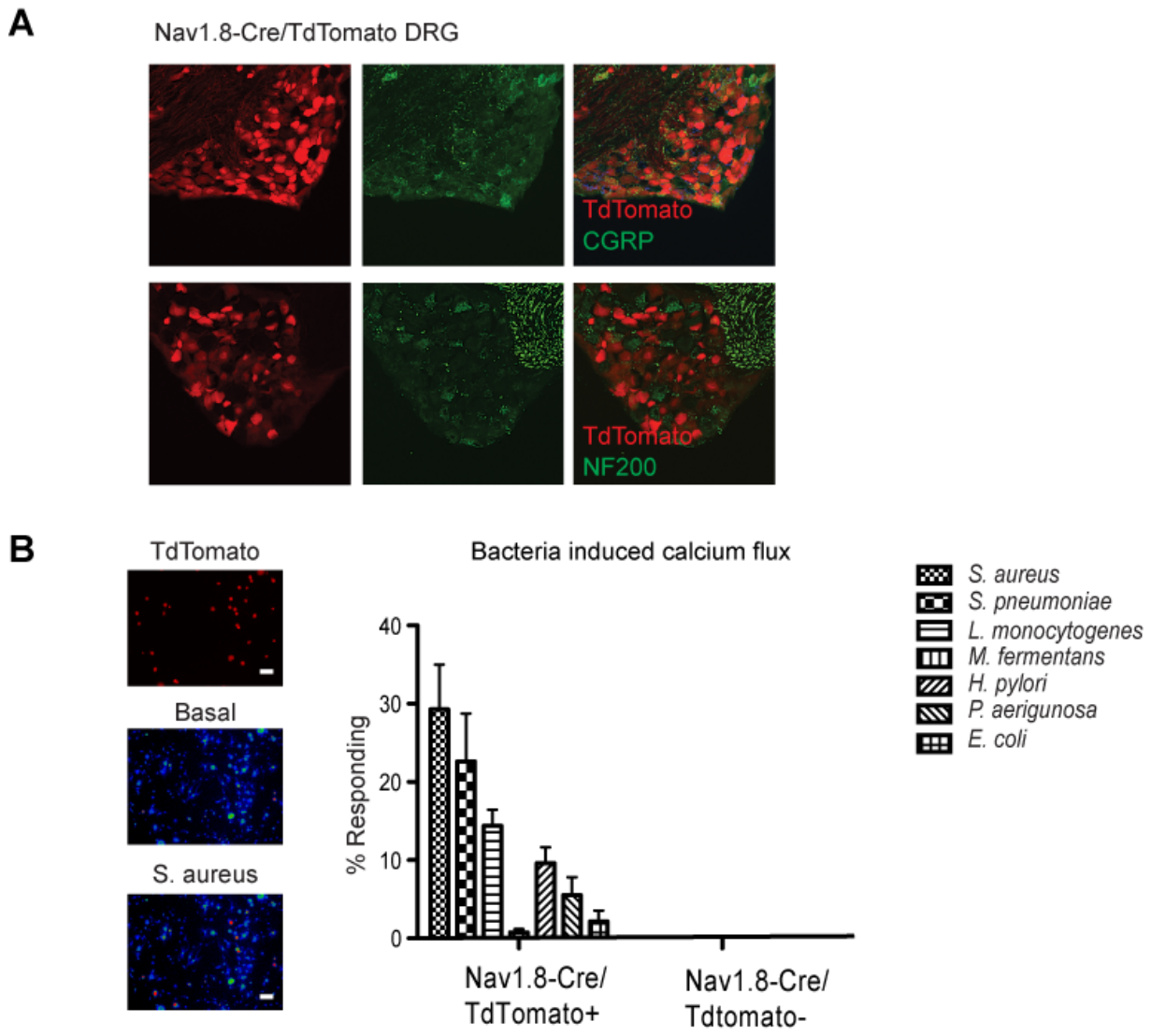

Supplemental Figure 10. Heat-killed bacteria induce calcium flux in Nav1.8 lineage DRG neurons and not other DRG neuronal sub-types. (A) Nociceptor-specific Nav1.8-Cre were bred with TdTomato reporter mice to generate Nav1.8-Cre/TdTomato mice. Lumbar DRG sections were immunostained for CGRP (millipore, 1:1000, green) and for neurofilament-200 (Sigma, 1:1000, green). $CGRP^+$ peptidergic neurons were within the Nav1.8-Cre/TdTomato subset, while most $NF200^+$ A-fibers were excluded from the Nav1.8-Cre/TdTomato subset. **(B)** Representative calcium imaging field of TdTomato expressing neurons, with cells before (basal) and after application of hk-*S. aureus*. All *S. aureus* responding neurons were also $TdTomato^+$. Bar graph shows quantification of Nav1.8-Cre/$TdTomato^+$ and Nav1.8-Cre/$TdTomato^-$ DRG neurons responding to different hk-bacteria strains (10^7 CFU/ml). Shown are proportion of responding DRG neurons within each Tdtomato subset/field. Error bars, mean±s.e.m.

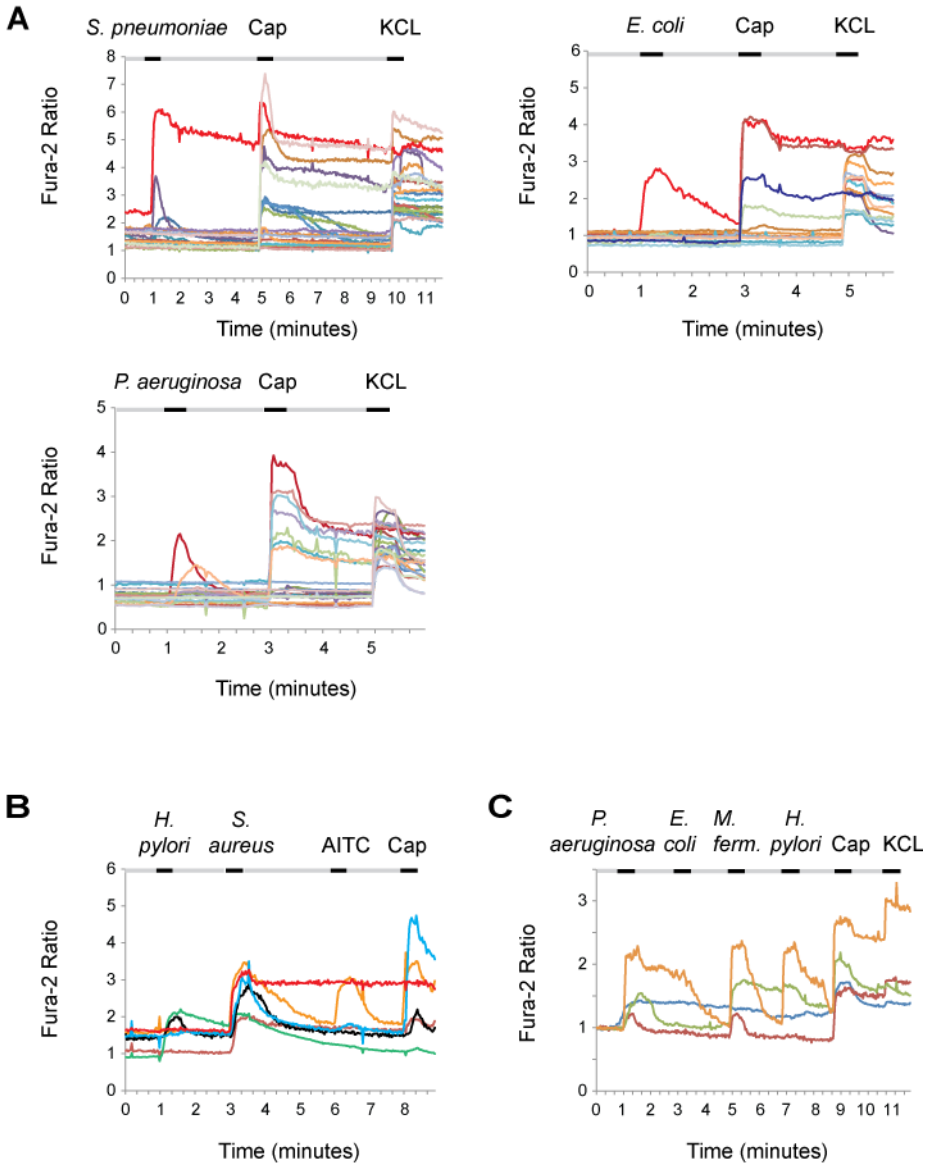

Supplemental Figure 11. Hk-bacteria strains induce differential activation of nociceptor subsets.
All hk-bacteria were applied at 10^7 CFU/ml. **(A)** Sequential application (black) with buffer washout (gray) of hk-*S. pneumoniae*, capsaicin (1 µM), KCl (40 mM) induces activation of a subset of capsaicin responsive DRG neurons (representative ratiometric traces shown). Neuronal responses to hk-*E. coli* and hk-*P. aeruginosa* are also shown. **(B)** DRG neurons subjected to sequential application and washout of hk-*H. pylori*, hk-*S. aureus*, allyl isothiocyanate (100 µM), and capsaicin (1 µM). Representative calcium traces show neurons responding hk-*S. aureus* but not to hk-*H. pylori*. **(C)** Sequential application and washout of hk-*P. aerigunosa*, hk-*E. coli,* hk-*M. fermentans,* hk-*H. pylori*, capsaicin (1 µM), and KCL (40 mM) shows representative traces of neurons responding to some bacteria, but not others. These results indicate multiple ligands mediating nociceptor calcium flux within different bacteria.

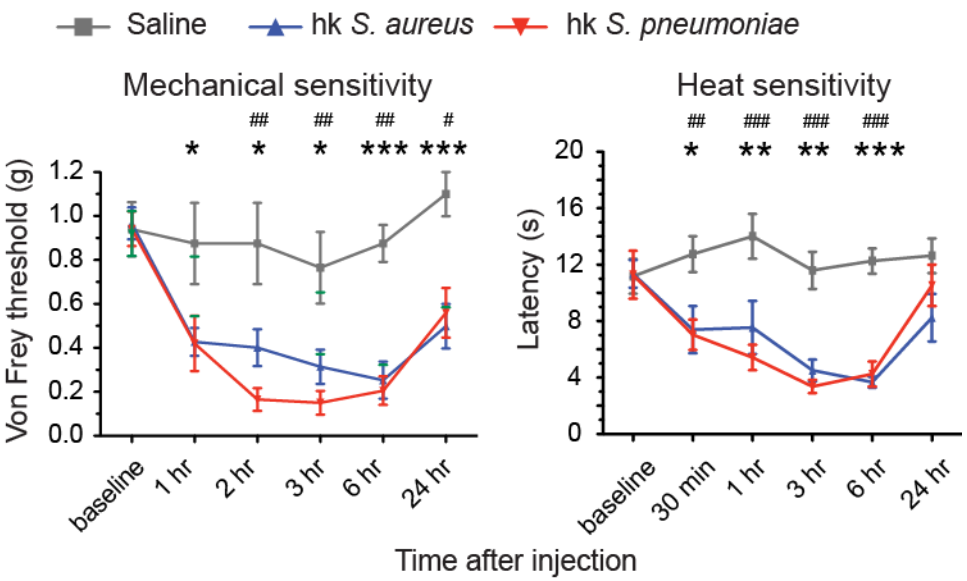

Supplemental Figure 12. Hk-*S. aureus* and hk-*S. pneumoniae* injection induce sustained mechanical and heat hypersensitivity.
Left, Mechanical sensitivity following injection of 10^8 CFU hk-*S. pneumoniae* (n=6; p=0.0217) or 10^8 CFU hk-*S. aureus* (n=16; p=0.0016) compared to saline (n=8). Heat sensitivity following injection of 10^8 CFU hk-*S. pneumoniae* (n=7, p=0.0005), or 10^8 CFU hk-*S. aureus* (n=7, p=0.026) vs. saline (n=6). Two-way RM ANOVA with Bonferroni post-tests: hk-*S. aureus*, #p<0.05; ##p<0.01; ###p<0.001. hk-*S. pneumonia*, *, p<0.05, **, p<0.01, ***, p<0.001. Error bars, mean±s.e.m.

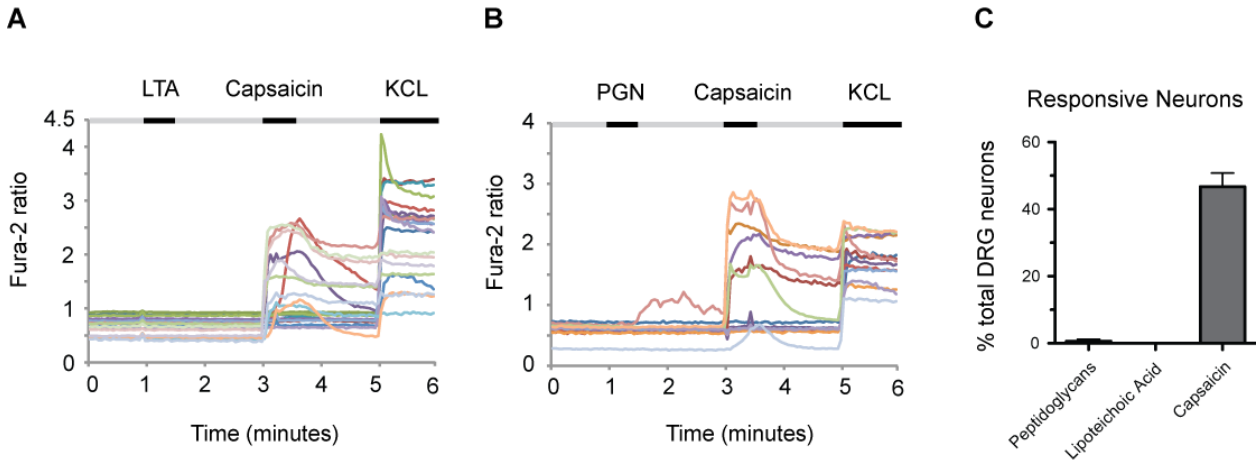

Supplemental Figure 13. *S. aureus* derived LTA and PGN do not induce significant calcium flux in DRG neurons. Sequential application (black) and buffer washout (gray) of *S. aureus* derived lipoteichoic acid (LTA, 1 µg/mL), *S. aureus* derived peptidoglycan (PGN, 1 µg/mL), capsaicin (1 µM) and KCL (40 mM), showing neurons responding to capsaicin but not to LTA or PGN. **(A-B)** Representative Fura-2 Ca^{2+} ratiometric traces in fields of neurons for PGN, or LTA, followed by capsaicin and KCL. **(C)** Quantification of proportion of DRG neurons responding to PGN, LTA, or Capsaicin out of total KCL responsive neurons. Error bars, mean± s.e.m.

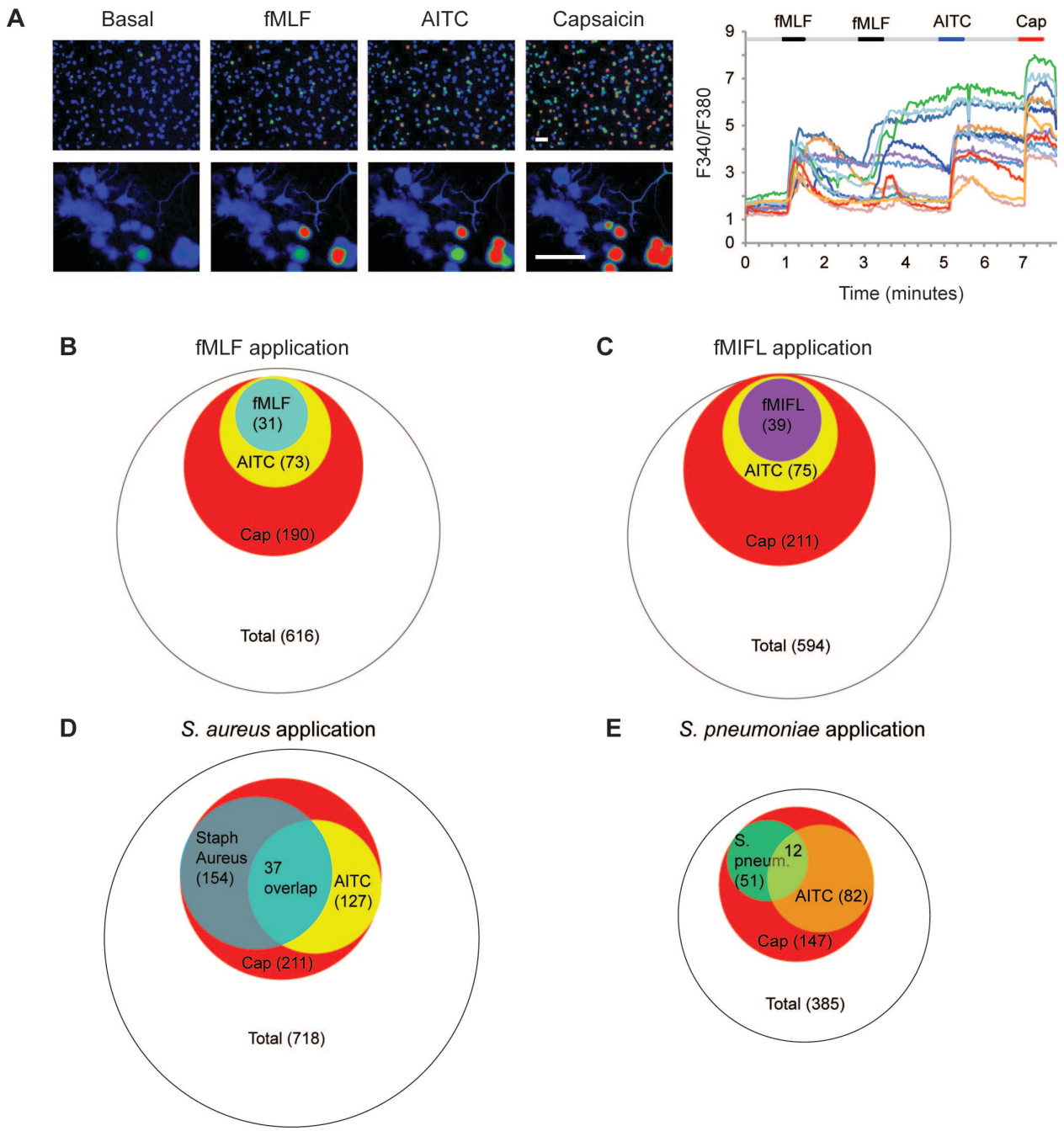

Supplemental Figure 14. Formyl peptides activate a subset of AITC responsive neurons, while heat-killed bacteria activate a larger nociceptor subset.
(A) Low and high magnification of Fura-2 ratiometric images of DRG neurons after application of fMLF (1 µM), allyl isothiocyanate (AITC, 100 µM), capsaicin (1 µM). Scale bars, 100 µm. Representative Fura-2 traces are on left. **(B-C)** Venn diagrams of DRG neuronal responsive cells, showing that all neurons responding to *E. coli* derived fMLF or *S. aureus* derived fMIFL are also AITC, capsaicin responsive. **(D-E)** Venn diagrams show neurons responding to hk-*S. aureus* or hk-*S. pneumoniae*, indicating that hk-bacteria induce a larger subset of neuronal responses than formylated peptides.

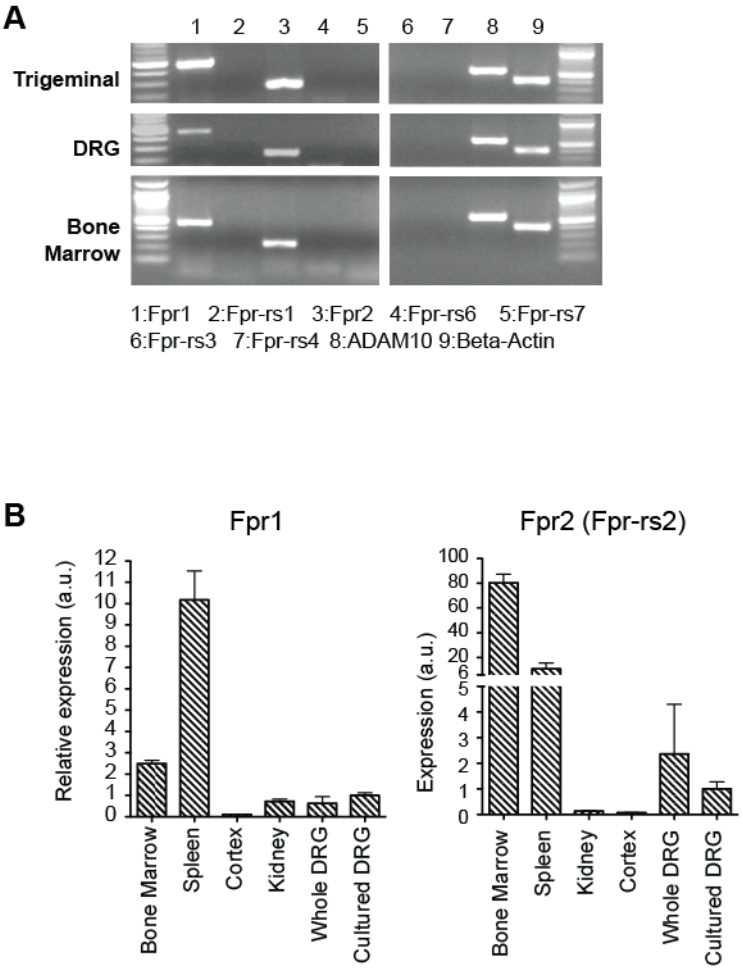

Supplemental Figure 15. Fpr1 and Fpr2, but not other Fprs, are expressed in sensory ganglia.

(A) RT-PCR of Fpr1, Fpr-rs1, Fpr2 (Fpr-rs2), Fpr-rs6, Fpr-rs7, Fpr-rs3, Fpr-rs4, ADAM10, β-Actin from cDNA synthesized from mouse trigeminal ganglia, dorsal root ganglia, and bone marrow RNA. Expression of Fpr1, Fpr2, ADAM10 were detected, but not other Fprs. **(B)** Quantitative PCR for Fpr1 and Fpr2 from mouse bone marrow, spleen, cortex, kidney, whole DRG and cultured DRG neuron-derived cDNA. Fpr1 and Fpr2 are expressed in immune organs (bone marrow, spleen) and DRG. Error bars, mean±s.e.m.

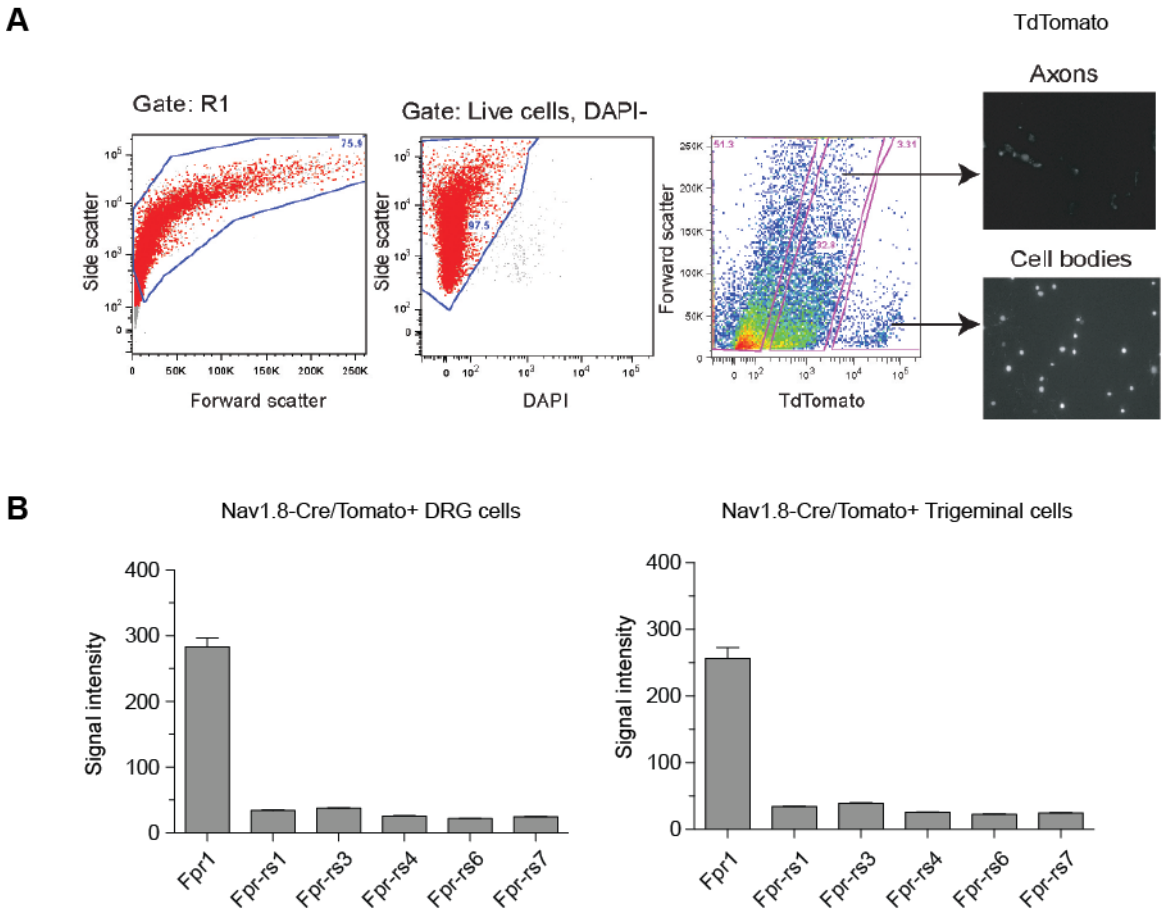

Supplemental Figure 16. FACS purified Nav1.8-Cre/TdTomato$^+$ neurons express Fpr1. **(A)** DRG from adult Nav1.8-Cre/TdTomato mice were dissected, dissociated, and fluorescence activated cell sorting (FACS) purified: shown is gating strategy for live DRG cells by exclusion of DAPI$^+$ cells followed by gating on neuronal cell bodies, which harbored high Tdtomato$^+$ fluorescence, instead of axons, which harbored low Tdtomato$^+$ fluorescence. Following sorting of cell bodies, neurons are found to be highly pure, as shown by microscopy. The same sorting strategy was used for trigeminal and nodose purification (Figure 6). **(B)** RNA from FACS purified Nav1.8-Cre/TdTomato$^+$ DRG neurons (n=3 samples) and Nav1.8-Cre/TdTomato$^+$ trigeminal neurons (n=4 samples) were subject to microarray analysis. Normalized expression signal intensities are given for Fpr1 (probeset 10448127), Fpr-rs1 (probeset 10442098), Fpr-rs3 (probeset 10448168), Fpr-rs4 (probeset 10442104), Fpr-rs6 (probeset 10448148), and Fpr-rs7 (probeset 10448146). Error bars, mean±s.e.m.

Note: The Fpr2 (Fpr-rs2) probeset was not available on this genechip (Affymetrix Mouse Gene ST 1.0), and so we do not state its presence or absence in sorted Nav1.8-Cre/TdTomato$^+$ cells.

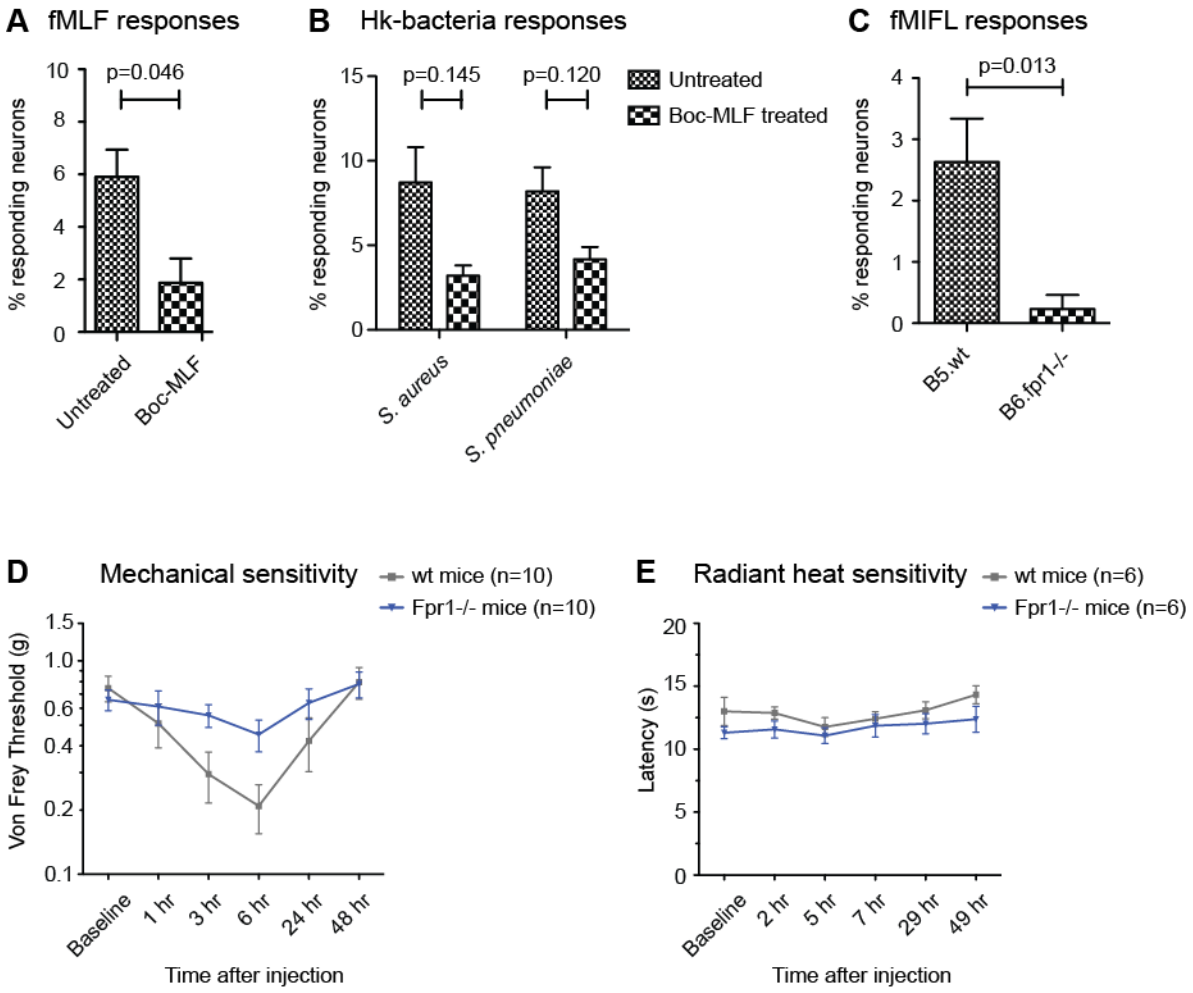

Supplemental Figure 17. FPR1 mediates nociceptor responses to fMIFL and induction of hyperalgesia following fMIFL injection.
(A-B) DRG neurons were treated with buffer alone or with Fpr1 antagonist Boc-MLF (10 μM) for 10 minutes prior to application of fMLF (1 μM), hk-*S. aureus* (10^7 CFU/ml) or hk-*S. pneumoniae* (10^7 CFU/ml). Fura-2 ratiometric imaging determined neurons responding by calcium flux. Boc-MLF decreases the proportion of neurons responding to fMIFL and hk-bacteria (p-value, t-test). **(C)** DRG neurons from B6.WT and B6.Fpr1-/- mice were analyzed in parallel for calcium flux responses to fMIFL (1 μM) by Fura-2 ratiometric imaging. The proportion of fMIFL is significantly decreased in $Fpr1^{-/-}$ cultures (p-value, t-test). **(D-E)** fMIFL induced mechanical hypersensitivity is significantly reduced in $Fpr1^{-/-}$ mice. Following injection of fMIFL (2 nmoles), mechanical hypersensitivity was significantly reduced in $Fpr1^{-/-}$ compared to WT mice (p=0.044, Two-way RM ANOVA). Radiant heat sensitivity was not changed by fMIFL injection in both B6.$Fpr1^{-/-}$ and B6.WT mice. Error bars, mean±s.e.m.

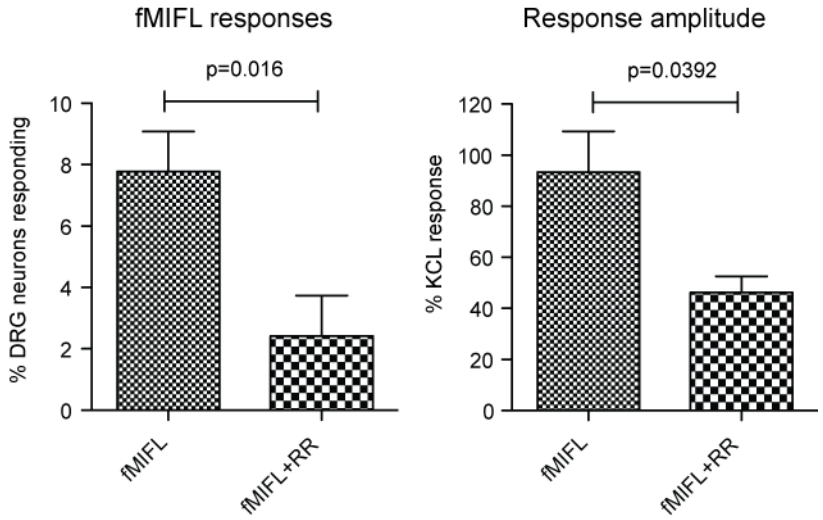

Supplemental Figure 18. Ruthenium Red significantly reduces the proportion and amplitude of fMIFL neuronal responses.
fMIFL (1 mM) was applied to cultured DRG neurons in the presence or absence of Ruthenium Red (RR, 10 mM), and calcium flux responses quantified by Fura-2 ratiometric imaging. **(A)** The proportion of neurons responding to fMIFL by calcium flux is significantly decreased in the presence of RR (p-value, t-test). Out of total DRG neurons, 18/184 responded to fMIFL by calcium flux, while 9/212 responded to fMIFL+RR. **(B)** The amplitude of fMIFL induced Calcium flux (Fura-2 ratio) was normalized to peak responses to KCl (40 mM). In the presence of Ruthenium Red, fMIFL response amplitudes were significantly decreased. P-value, t-test. Error bars, mean±s.e.m.

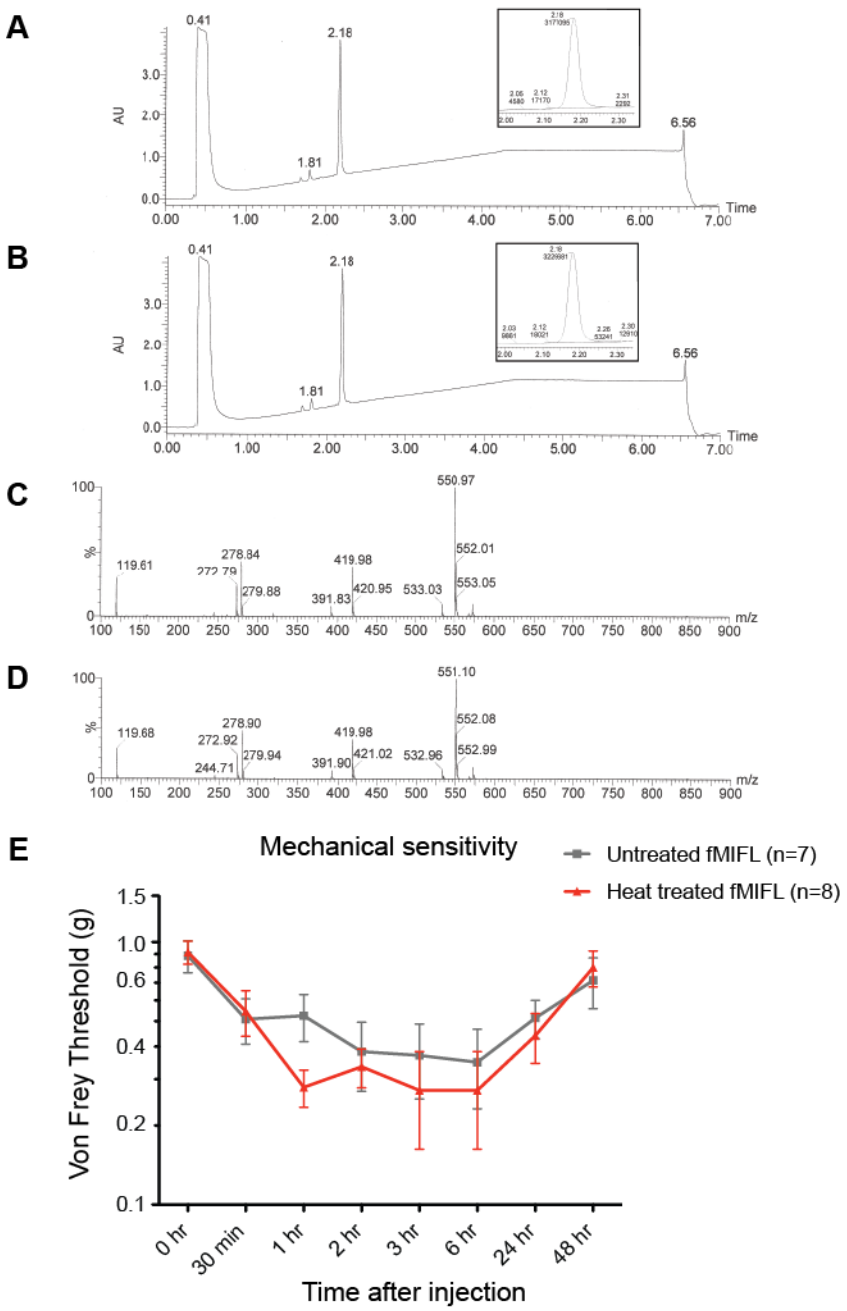

Supplemental Figure 19. Heat treatment does not alter the composition of fMIFL or its ability to induce mechanical hyperalgesia. (A-D) LC-MS analysis of fMIFL before and after heat treatment. HPLC chromatograms (λ= 220 nm) of untreated fMIFL (**A**) and after heat treatment for 100°C for 30 minutes (**B**), with the integration of the peak at 2.81 mins as the insert. The peak at 0.41 mins is the DMSO solvent peak. The peak at 2.18 mins is the peak corresponding to fMIFL with a minor unknown peak at 1.81 mins. The integration of the peak at 2.18 mins does not change after the heat treatment. ESI+ spectra of the 2.81 mins peak in untreated fMIFL (**C**) and fMIFL after heat treatment (**D**) were confirmed to be fMIFL. **(E)** Mice were injected with untreated fMIFL (n=7, 2 nmoles) or heat-treated fMIFL (n=8, 2 nmoles) show no significant differences in mechanical hypersensitivity (p=0.856, Two-way RM ANOVA).

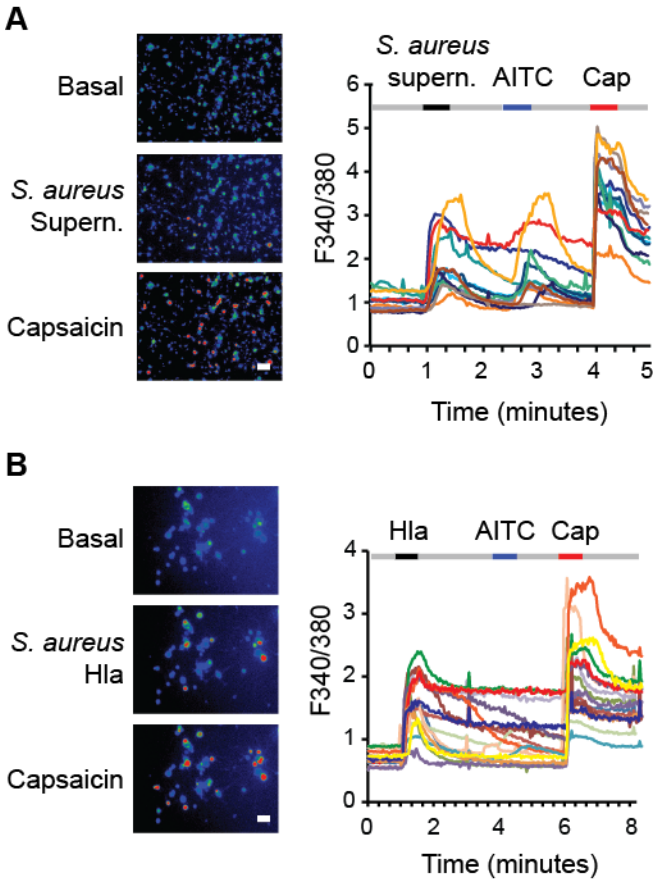

Supplemental Figure 20. S. aureus supernatant and the secreted toxin alpha-hemolysin (Hla) causes calcium flux in DRG neurons.
(A) *S. aureus* supernatant (5% in SES), containing bacteria-secreted factors, induces calcium flux in DRG neurons, of which some respond subsequently to AITC and Capsaicin. **(B)** Hla (10 μg/mL) application induces an immediate calcium flux in subset of DRG neurons on short exposure that is able to be washed out by buffer. Some Hla responsive neurons also responded to AITC, while the majority respond to capsaicin.

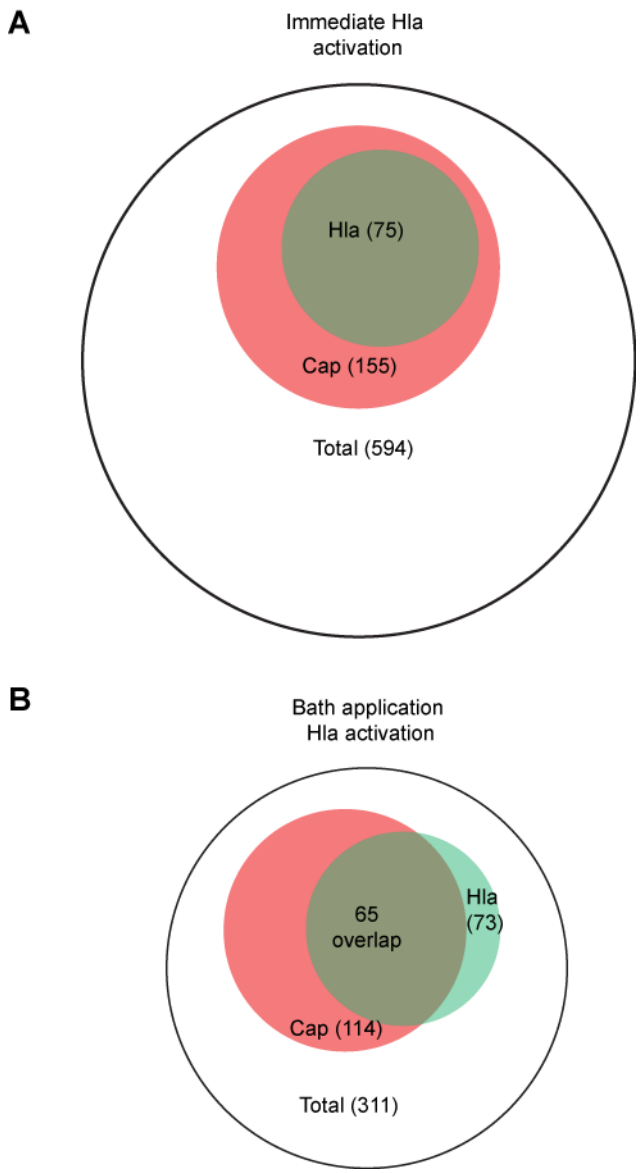

Supplemental Figure 21. Hla responsive DRG neurons are within capsaicin responsive subsets.

(A) Venn diagrams of neuronal responses to immediate application of Hla (10 μg/mL), buffer washout, and capsaicin (1 μM). All Hla responsive cells were also capsaicin responsive. **(B)** Venn diagrams showing Calcium flux responsiveness of DRG neurons from bath application of Hla (10 μg/mL). Capsaicin (1 μM) was applied after 24 minutes of Hla application. The majority of Hla responsive cells also responded to capsaicin.

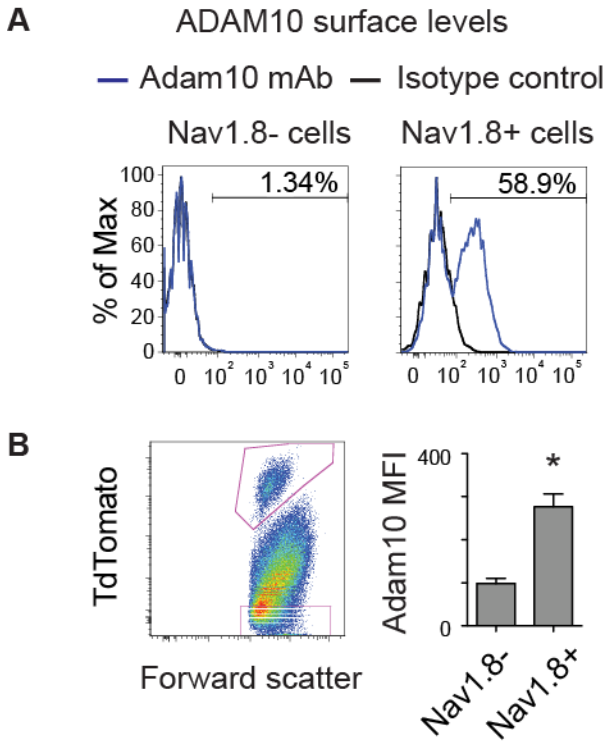

Supplemental Figure 22. ADAM10 is expressed on the surface of a subset of Nav1.8-Cre/Tdtomato+ neurons.
(A) Nav1.8-Cre/Tdtomato DRG cells stained with isotype control or anti-ADAM10 antibody analyzed by flow cytometry (see Supplemental Figure 16 for general neuron gating strategy). Histograms show 58.9% Tdtomato^{+} cells expressed surface ADAM10, while there is little staining with isotype control antibody. **(B)** Nav1.8-Cre/TdTomato^{+} cell bodies show significantly higher mean fluorescence intensity (MFI) than Tdtomato^{-} cells (gated cells on left, MFI on right, n=3, *, $p<0.05$, t-test). Error bars, mean±s.e.m.

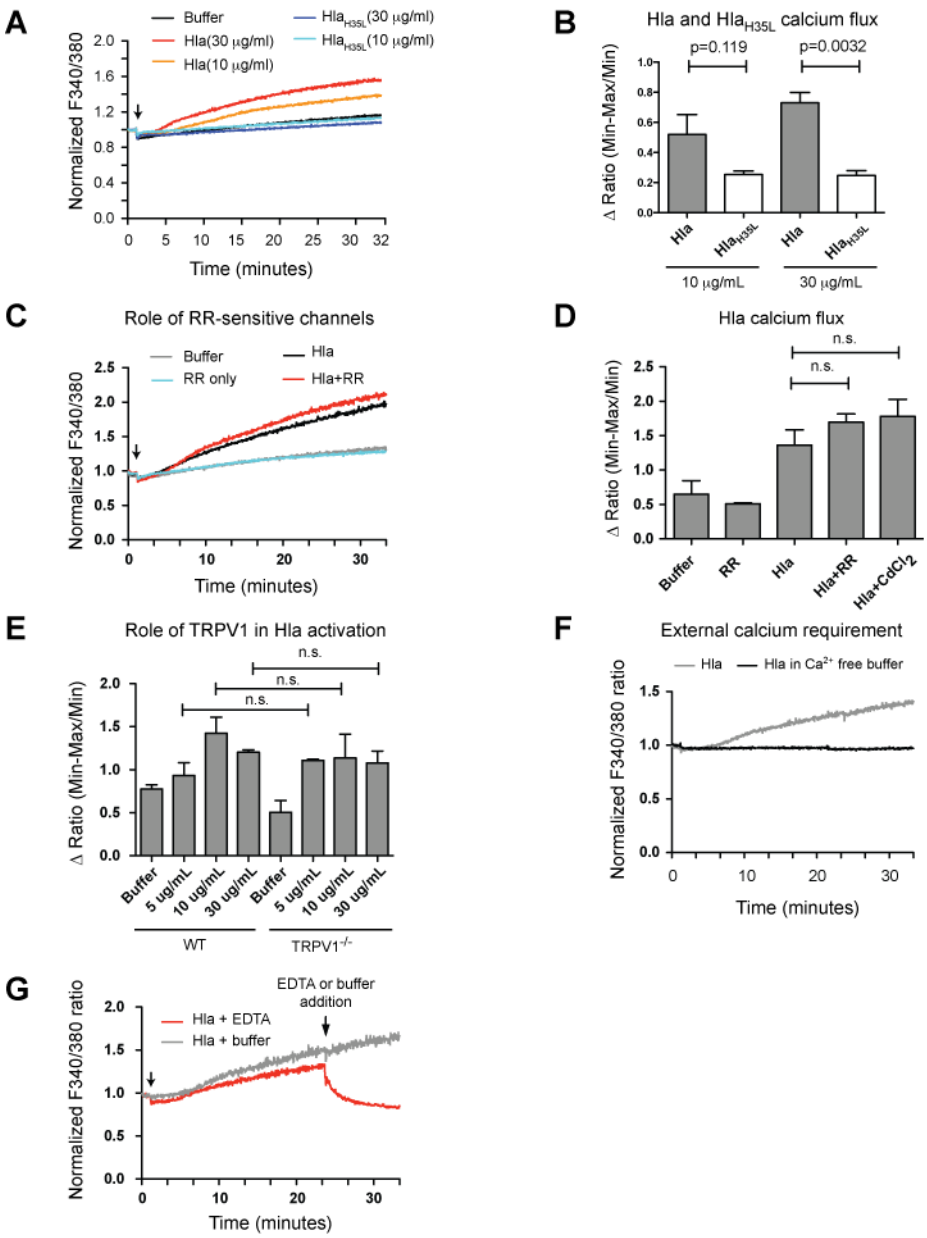

Supplemental Figure 23. Mechanism of Hla mediated calcium flux in DRG neurons. Calcium flux in DRG neurons were analyzed by whole-well Fura-2 ratiometric imaging. **(A)** Average ratiometric traces of calcium flux following application (arrow) of buffer (HBSS), Hla or mutant Hla$_{H35L}$ (10 μg/mL, 30 μg/mL). **(B)** Significantly less DRG calcium flux occurs for Hla$_{H35L}$ relative to WT Hla (p-values, t-test). **(C-D)** Hla (30 μg/mL) was applied with or without Ruthenium Red (RR, 10 uM). Normalized ratiometric traces show induction of calcium flux in the presence and absence of RR. Quantification shows no significant differences between Hla, Hla+RR (10 μM) and Hla+$CdCl_2$ (50 μM). **(E)** Hla calcium flux does not differ between WT and TRPV1$^{-/-}$ DRG cultures (5, 10, 30 μg/mL). **(F-G)** Hla (30 μg/mL) induced calcium flux is absent in calcium-free buffer, and addition of the chelator EDTA (5 mM) caused a decrease in Hla calcium flux. In all graphs, traces are average of triplicate wells; arrows, time of ligand application. P-values, t-test. Error bars, mean±s.e.m.

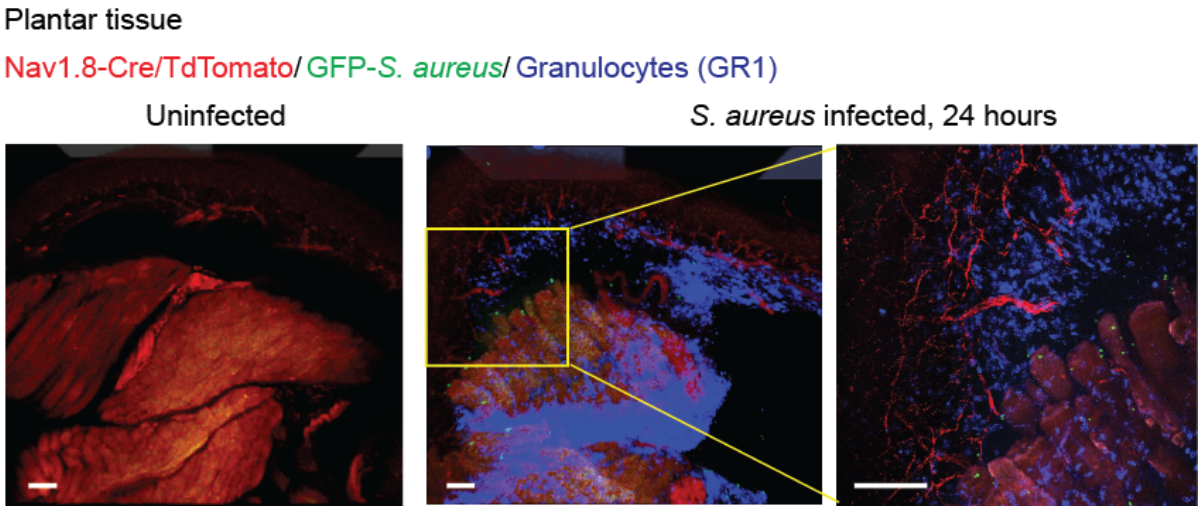

Supplemental Figure 24. Gr1^{+} cells are found in close proximity with nociceptor nerve fibers in *S. aureus* infected tissues and co-culture of neutrophils/macrophages with DRG neurons.
Nav1.8-Cre/TdTomato mice were infected with GFP-LAC/USA300, paw tissue collected 24 hours post-infection, fixed and cryosectioned. Sections were stained with anti-GR1, followed by Alexa 647 anti-Rat IgG. Confocal microscopy shows close apposition of GR1^{+} granulocytes (which includes neutrophils and monocytes) with Nav1.8-Cre/TdTomato^{+} nociceptive nerve fibers. Scale bars, 100 μm.

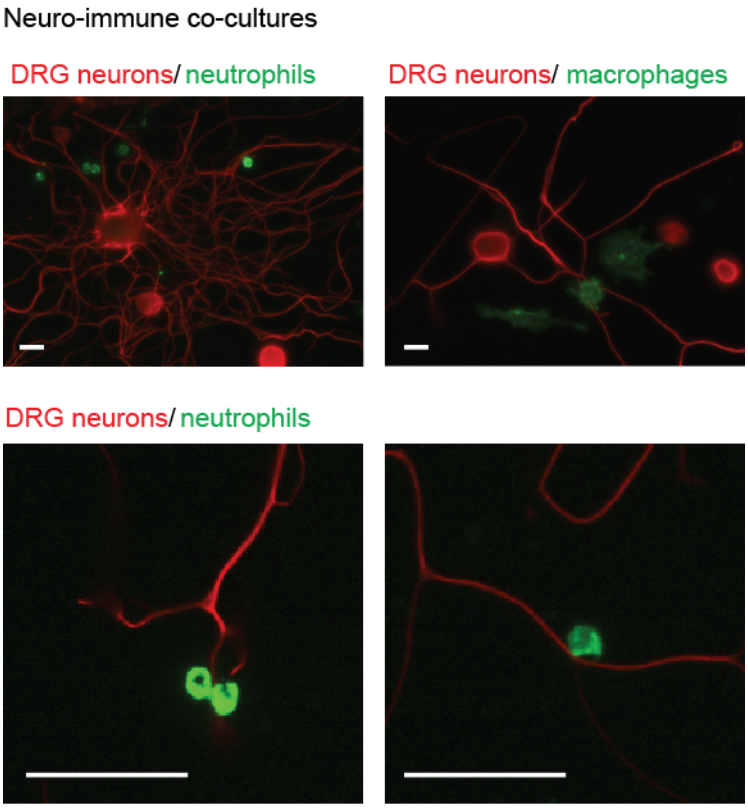

Supplemental Figure 25. Neutrophils and macrophages are found in close proximity with neuritis in co-culture with DRG neurons.
DRG neurons were co-cultured with bone marrow-isolated neutrophils (top left and bottom panels) or bone marrow-derived macrophages (top right) for 16 hours *in vitro*. Fixed co-cultures were stained with mouse anti-βIII-tubulin and rat anti-CD11b, followed by Alexa 488 goat anti-mouse IgG (green) and Alexa 568 goat anti-rat IgG (red). Imaging by epifluorescence microscopy. Scale bars, 10 μm.

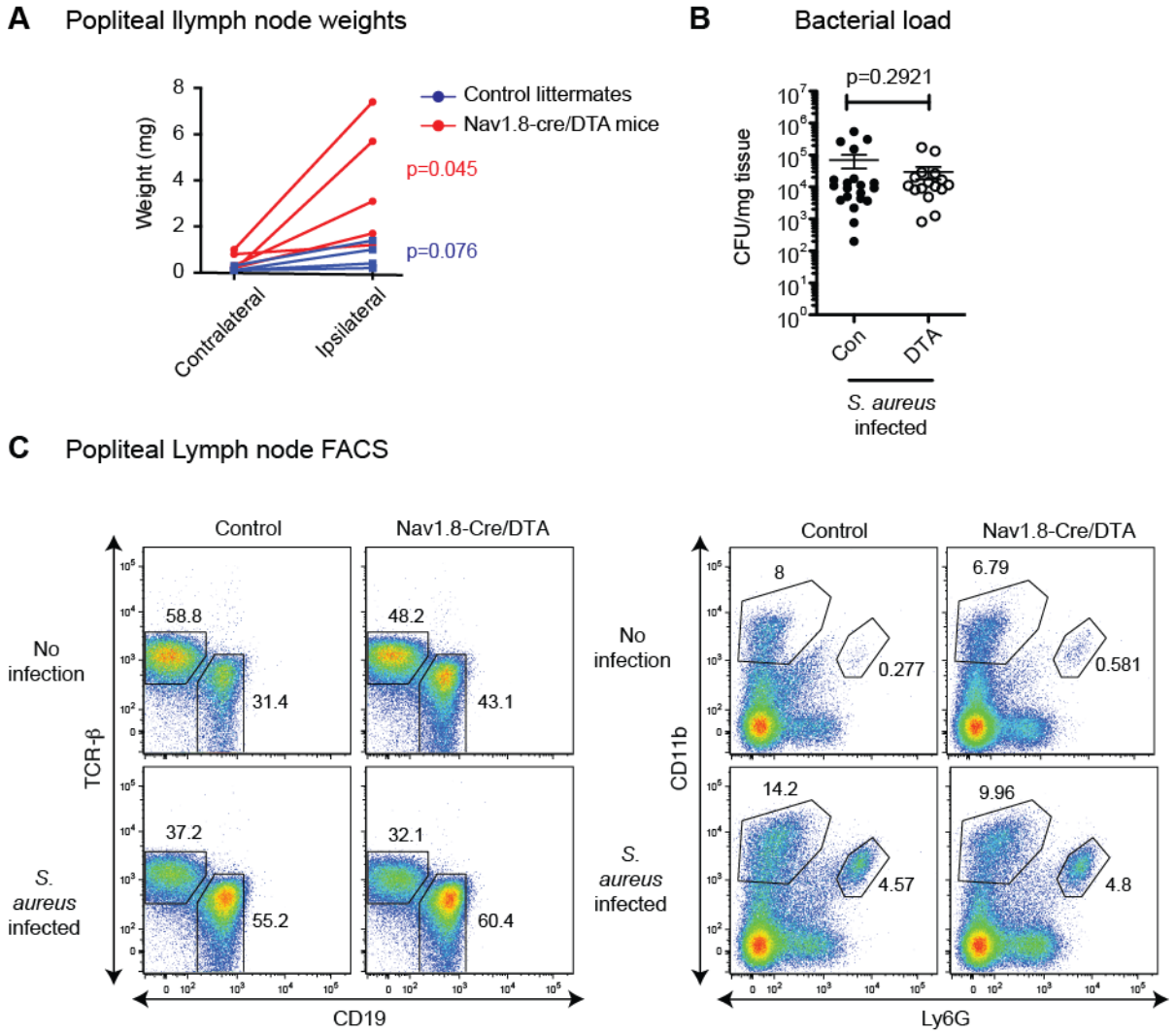

Supplemental Figure 26. Popliteal lymph node weight, bacterial load, and lymph node FACS in mice post-*S. aureus* infection. Nav1.8-Cre/DTA and control littermates infected with *S. aureus* ($5x10^6$ CFU) were analyzed 24 hours later. **(A)** Nav1.8-Cre/DTA mice (red) show significant differences between contralateral and ipsilateral draining popliteal lymph node weights following infection but not controls (blue) (p-values, unpaired t-test). **(B)** Bacterial load in infected tissues did not differ significantly between Nav1.8-Cre/DTA, control littermates. P-value, t-test. Error bars, mean±s.e.m. **(C)** Representative FACS of popliteal lymph nodes from uninfected and infected Nav1.8-Cre/DTA or control littermates. Cells were stained with a combination of TCR-β, CD19, CD11b, Ly6G, Ly6C antibodies. Shown are representative gates for T cells ($TCR\beta^+CD19^-$), B cells ($TCR\beta^-CD19^+$), neutrophils ($CD11b^+Ly6G^+$) and myeloid cells that are not neutrophils ($CD11b^+Ly6G^-$). These data in combination with cell counts by hemocytometer were used to calculate specific numbers of lymph node subsets. We found that while overall cellularity increased in Nav1.8-Cre/DTA mice following infection, no particular lymphoid or myeloid cell-type showed dramatic changes in proportion but rather there was a general increase in T, B, and monocyte/macrophage populations (Fig. 5e).

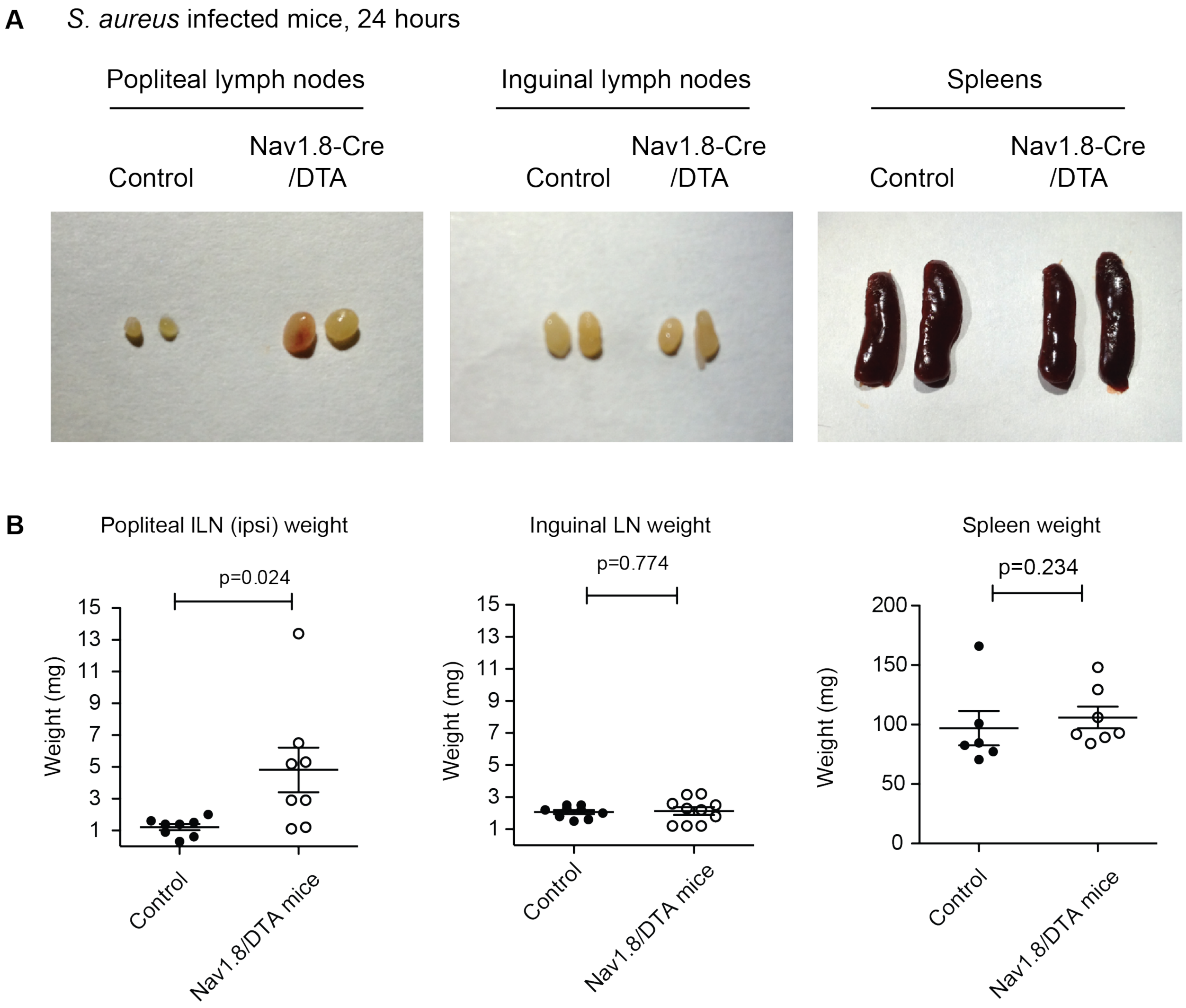

Supplemental Figure 27. Draining popliteal but not inguinal lymph nodes or spleens differ in size and weight following *S. aureus* infection of Nav1.8-Cre/DTA and control mice. **(A)** Representative images of ipsilateral popliteal lymph nodes, inguinal lymph nodes, and spleens from *S. aureus* infected animals. **(B)** Statistical comparison of weights of draining popliteal lymph nodes, inguinal lymph nodes, and spleens from infected control vs. Nav1.8-Cre/DTA mice. P-values, t-test. Error bars, mean±s.e.m.

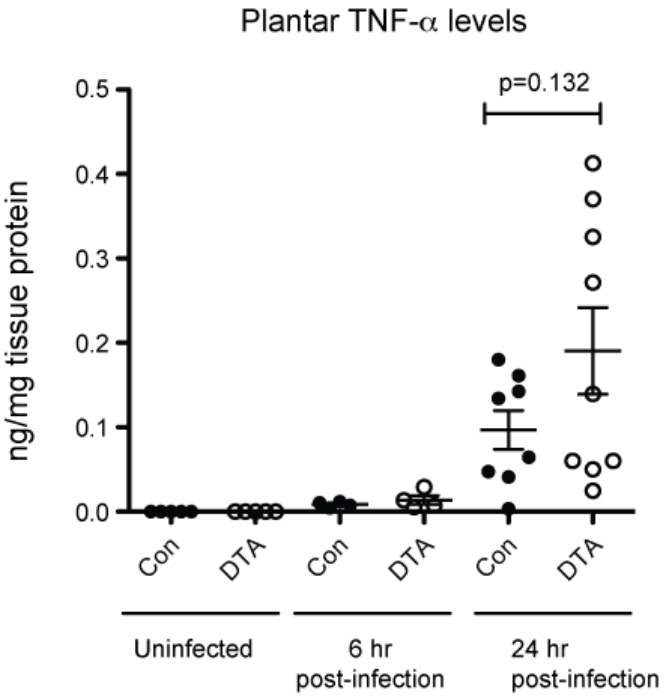

Supplemental Figure 28. Plantar TNF-α levels increase in Nav1.8-Cre/DTA mice following infection.

Plantar tissue was homogenized and analyzed for TNF-α levels (normalized to total protein in tissue) from Nav1.8-Cre/DTA and control mice either uninfected, infected for 6 hours, or infected for 24 hours with *S. aureus*. Individual mice are shown as data-points at each time-point. p-value, t-test. Error bars, mean±s.e.m.

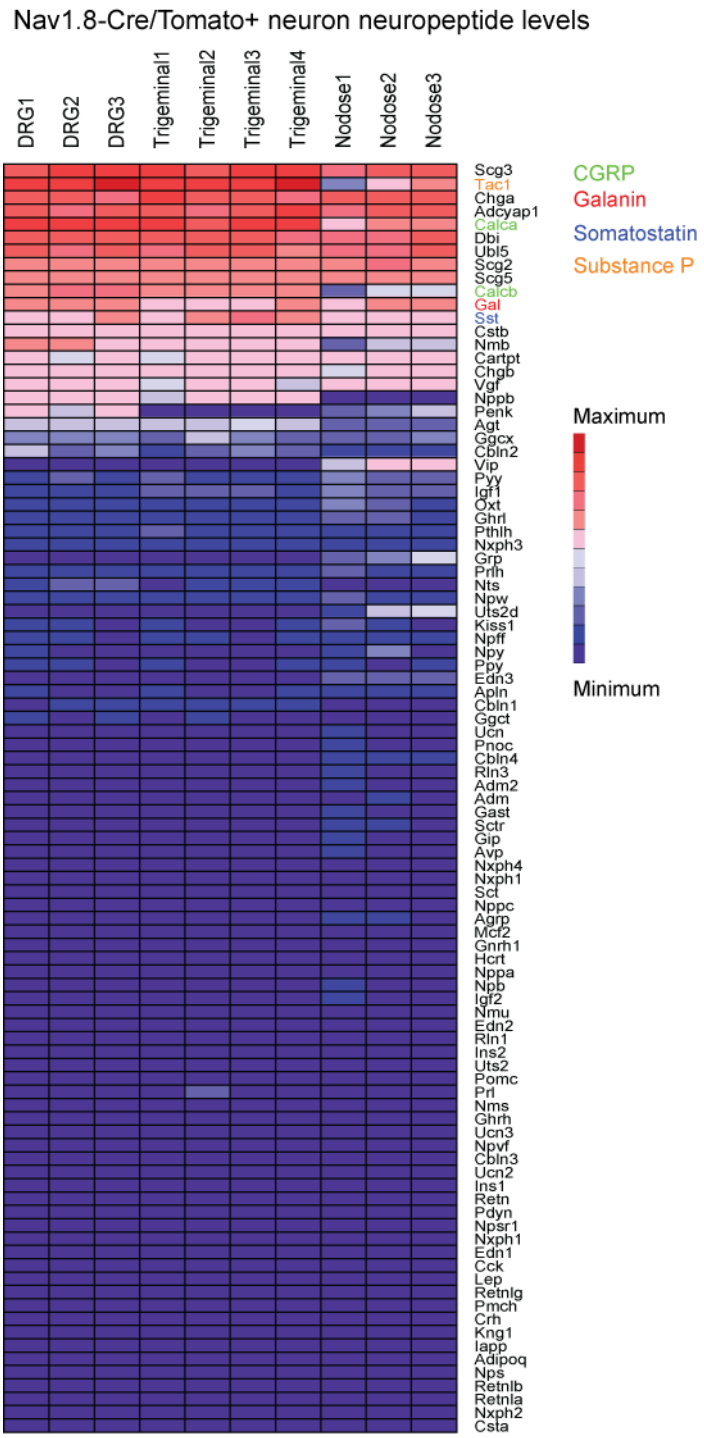

Supplemental Figure 29. Neuropeptide gene expression levels in Nav1.8-Cre/Tomato$^+$ DRG, trigeminal and nodose ganglion neurons. Nav1.8-Cre/Tomato$^+$ nociceptors were purified from DRG, trigeminal, and nodose ganglia, RNA extracted and subjected to microarray analysis. A list of neuropeptides was compiled (www.neuropeptides.nl), and corresponding average gene expression levels across all 3 nociceptor types were ranked from maximum to minimum by average expression, and represented as a heat-map. Genes encoding CGRP (green), galanin (red), somatostatin (blue), and substance P (orange) are highlighted.

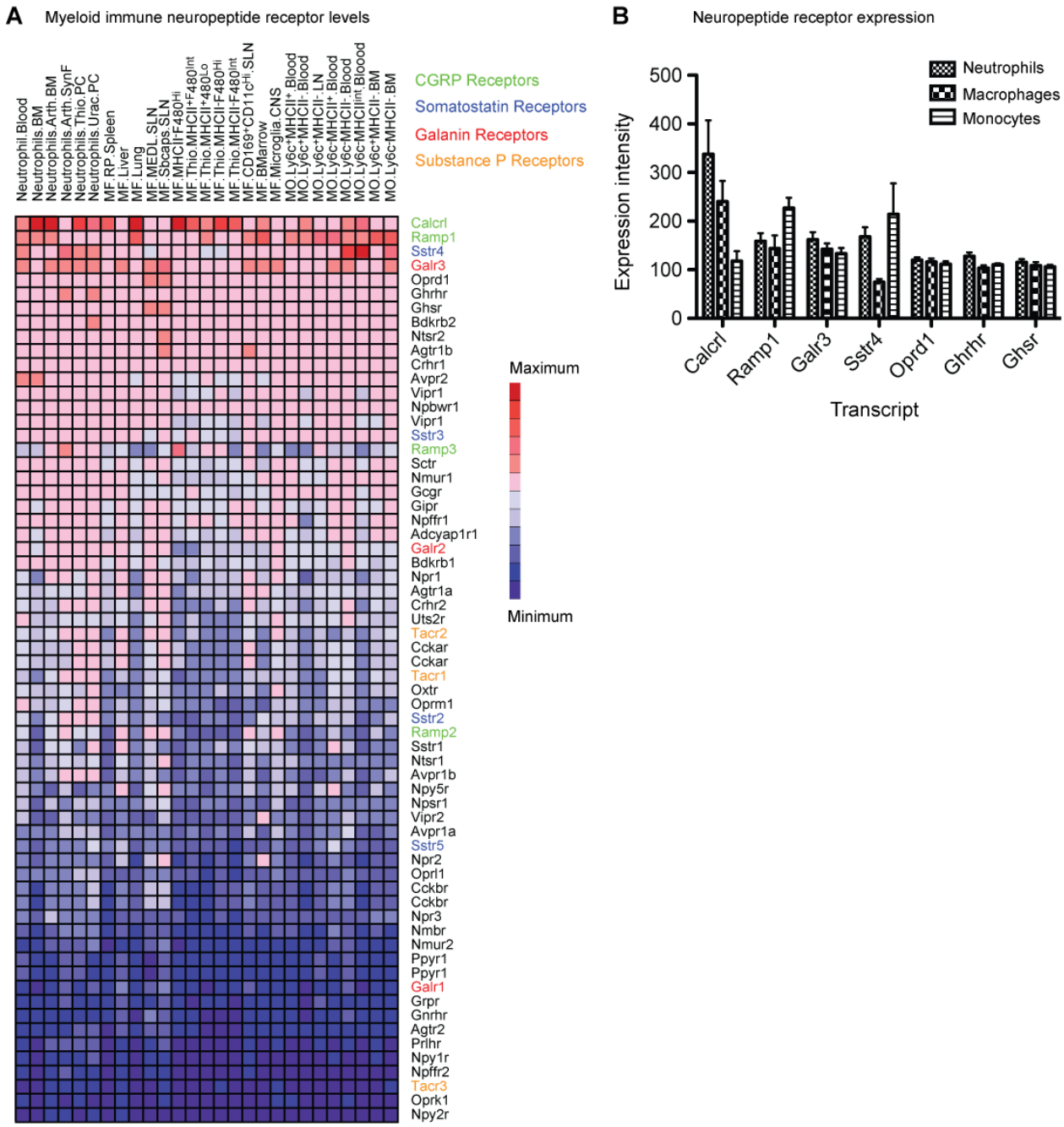

Supplemental Figure 30. Neuropeptide receptor gene expression levels in neutrophil, monocyte, and macrophage immune cell subsets. (A) ImmGen microarray datasets for different neutrophil, monocyte, macrophage subsets (names shown) were analyzed for average neuropeptide receptor gene expression levels, which were ranked from maximum to minimum and represented as a heat-map. Genes encoding receptors for CGRP (green), galanin (red), somatostatin (blue), and substance P (orange) are highlighted. **(B)** The top 7 neuropeptide receptors in myeloid immune cells as shown on the heat-map are plotted among neutrophil subsets, macrophage subsets, and monocyte subsets. Calcrl and Ramp1 bind CGRP, Galr3 binds galanin, and Sstr4 binds somatostatin. Error bars, mean±s.e.m.

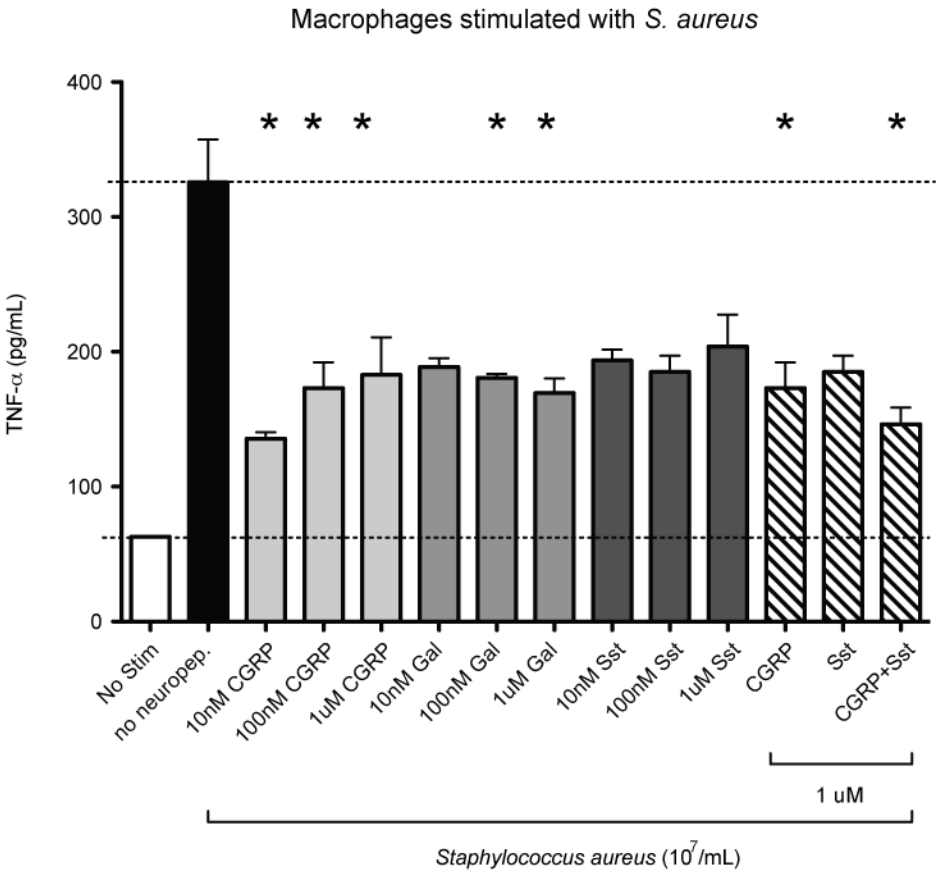

Supplemental Figure 31. CGRP, Galanin, and Somatostatin modulate macrophage TNF-α release in response to *S. aureus* stimulation.
Increasing concentrations of CGRP, Galanin (Gal) or Somatostatin (Sst) or combined CGRP and Sst were added in conjunction with hk-*S. aureus* (10^7 CFU/mL) to cultured bone marrow derived macrophages for 16 hours at 37°C. Supernatants were collected and analyzed for TNF-α by ELISA. (*, $p<0.05$, t-test, with *S. aureus* stimulated macrophages in the absence of neuropeptides, biological triplicates). Note: Some data are presented in Fig. 6, and this contains the full-range of concentrations tested. Triplicates, Error bars, mean±s.e.m.

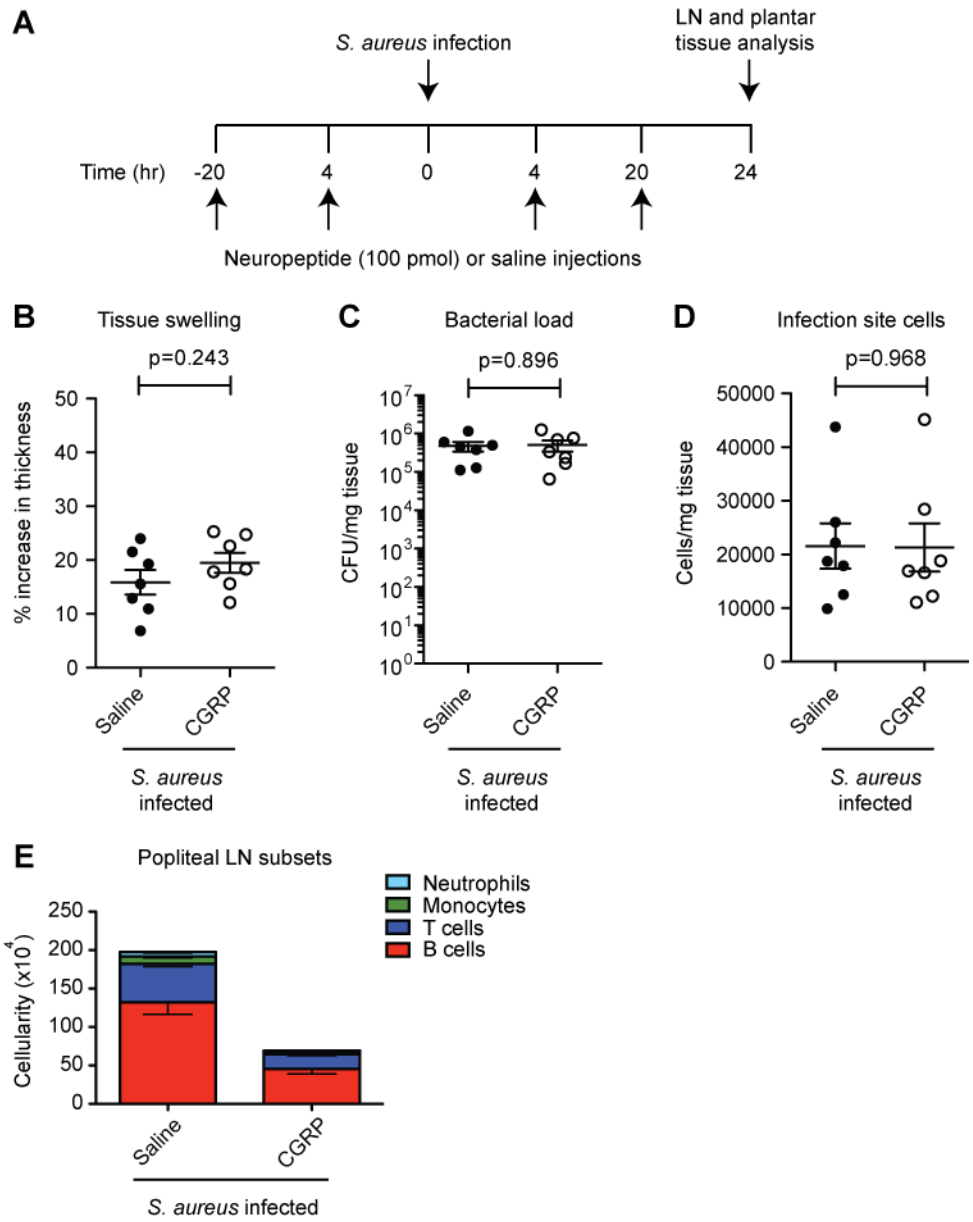

Supplemental Figure 32. CGRP injection does not affect *S. aureus* induced plantar inflammation but decreases lymphadenopathy.
(A) CGRP injection and *S. aureus* infection experimental scheme, followed by tissue collected and analysis 24 hours post-infection. **(B)** Tissue swelling as measured by % increase in thickness from baseline was not affected by CGRP injection (p-value, t-test). **(C)** Bacterial load at the infection site was not affected by CGRP injection (p-value, t-test). **(D)** Plantar tissue was analyzed for infection site cell numbers, which increase following infection and include neutrophils and monocytes. These did not differ with CGRP injection (p-value, t-test). **(E)** Draining popliteal lymph node cells counted for total cellularity showed significant decreases following CGRP injection (Fig. 6e). Here, these cells were analyzed by FACS for specific immune subsets, including neutrophil, monocyte, T cells, B cell which are plotted for saline and CGRP treated mice. Error bars, mean±s.e.m.

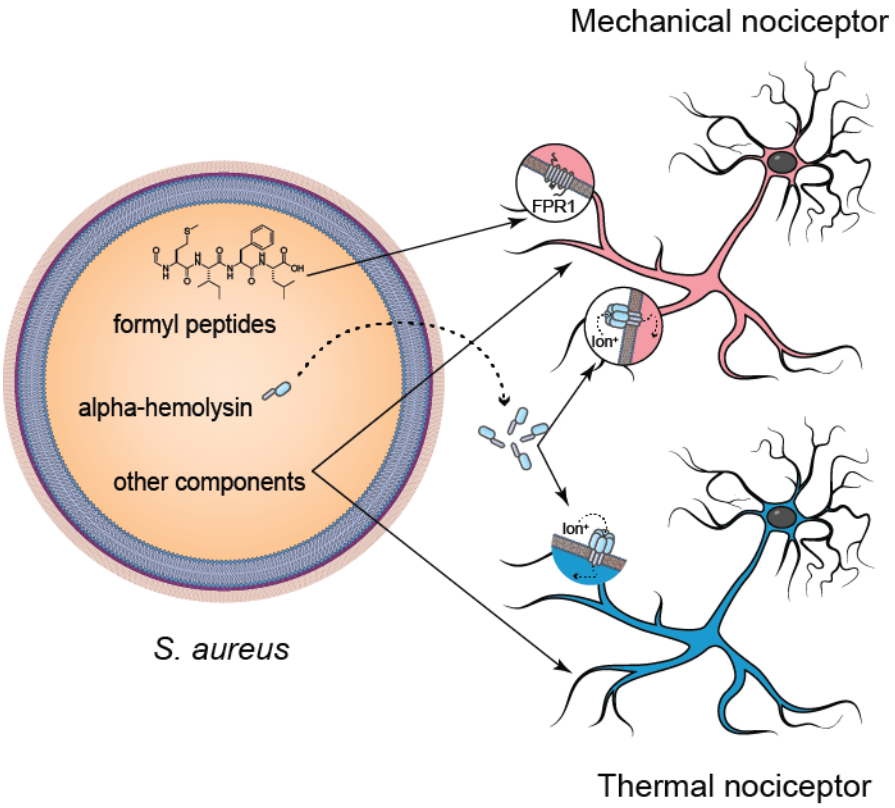

Supplemental Figure 33. Bacteria directly activate nociceptor neurons through distinct mechanisms.
Bacteria directly activate nociceptors through several distinct mechanisms: 1) N-formylated peptides, heat-stable components found in bacteria, activate FPR1 on a subset of nociceptor neurons that mediate mechanical but not heat hyperalgesia. 2) Hla, a pore-forming toxin that is heat-sensitive and secreted by *S. aureus*, binds to nociceptor cell membranes, and oligomerizes to form pores allowing ionic entry and depolarization. This is sufficient to induce mechanical and thermal hyperalgesia. 3) Other unidentified molecular components activate nociceptors that mediate mechanical and thermal hyperalgesia.